

Interactive Biogenic Emissions and Drought Stress Effects on Atmospheric Composition in NASA GISS ModelE

Elizabeth Klovenski¹, Yuxuan Wang¹, Susanne E. Bauer², Kostas Tsigaridis^{2,3}, Greg Faluvegi^{2,3}, Igor Aleinov^{2,3}, Nancy Y. Kiang², Alex Guenther⁴, Xiaoyan Jiang⁴, Wei Li¹, Nan Lin⁵

¹ Department of Earth and Atmospheric Sciences, University of Houston, Houston, TX, USA

² NASA Goddard Institute for Space Studies, New York, NY, USA

³ Center for Climate Systems Research, Columbia University, New York, NYC, USA

⁴ Department of Earth System Science, University of California – Irvine, Irvine, CA, USA

⁵ Ministry of Education Key Laboratory for Earth System Modeling, Department of Earth System Science, Tsinghua University, Beijing, China

Corresponding author: Yuxuan Wang (ywang246@central.uh.edu)

Key Points:

- A new method to capture regional changes of isoprene drought stress is implemented for global usage in NASA GISS ModelE and is evaluated at the MOFLUX Ameriflux site located in Missouri.
- The inclusion of isoprene drought stress from 2003-2013 leads to a ~2.7% reduction in global decadal average of isoprene emissions in ModelE with up to ~20% reduction in drought-stricken regions.
- The model-tuned parameterization of isoprene drought stress reduces the overestimation of ΩHCHO in the southeastern U.S and improves simulated O_3 during drought periods.

Abstract. Drought is a hydroclimatic extreme that causes perturbations to the terrestrial biosphere, and acts as a stressor on vegetation, affecting emissions patterns. During severe drought, isoprene emissions are reduced. In this paper, we focus on capturing this reduction signal by implementing a new percentile isoprene drought stress (y_d) algorithm in NASA GISS ModelE based on the MEGAN3 (Model of Emissions of Gases and Aerosols from Nature Version 3) approach as a function of a photosynthetic parameter ($V_{c,max}$) and water stress (β). Four global transient simulations from 2003-2013 are used to demonstrate the effect without y_d (Default_ModelE) and with online y_d (DroughtStress_ModelE). DroughtStress_ModelE is evaluated against the observed isoprene measurements at the Missouri Ozarks Ameriflux (MOFLUX) site during the 2012 severe drought where improvements in correlation coefficient indicate it is a suitable drought stress parameterization to capture the reduction signal during severe drought. The application of y_d globally leads to a decadal average reduction of ~2.7% which is equivalent to ~14.6 Tg yr⁻¹ of isoprene. The changes have larger impacts in regions such as the Southeast U.S.. DroughtStress_ModelE is validated using satellite ΩHCHO column from the Ozone Monitoring Instrument (OMI) and surface O_3 observations across regions of the U.S. to examine the effect of drought on atmospheric composition. It was found the inclusion of isoprene drought stress reduced the overestimation of ΩHCHO in Default_ModelE during the

44 2007 and 2011 southeastern U.S. droughts and lead to improvements in simulated O₃ during
45 drought periods. We conclude that isoprene drought stress should be tuned on a model-by-model
46 basis, because the variables used in the parameterization responses are relative to the land
47 surface model hydrology scheme (LSM) and the effects of y_d application could be larger than
48 seen here due to ModelE not having large biases of isoprene during severe drought.
49

50 **Plain Language Summary:** Severe drought stresses vegetation and causes reduced emission of
51 isoprene. We study the impact of including a new isoprene drought stress (y_d) parameterization
52 into NASA GISS ModelE called (DroughtStress_ModelE), which is specifically tuned for
53 ModelE. Inclusion of y_d leads to better simulated isoprene emissions at the MOFLUX site
54 during the severe drought of 2012, reduced overestimation of OMI satellite Ω HCHO
55 (formaldehyde column) and improved simulated O₃ (ozone) during drought.
56

57 **1. Introduction**

58 In present day conditions terrestrial ecosystems release about 1000 Tg C yr⁻¹ of biogenic
59 volatile organic compounds (BVOCs) into the atmosphere and there is an additional smaller
60 emission from marine ecosystems (Guenther *et al.* 2012). The majority of BVOCs emitted from
61 vegetation are isoprene and monoterpenes (Guenther *et al.* 2006; Guenther *et al.* 2012).
62 Representing over half of emitted BVOCs, isoprene is the dominant species globally with
63 reported ranges of 440-600 Tg C yr⁻¹ (Guenther *et al.* 2012) with high emission factors from
64 some, but not all, broadleaf trees including species of oak, willow, palm oil, and eucalyptus
65 (Benjamin *et al.* 1996; Geron *et al.* 2000). Isoprene is produced from carbon substrates generated
66 during photosynthesis and contributes to abiotic stress tolerance from water and temperature
67 stress (Loreto and Sharkey 1990; Monson *et al.* 2021). Isoprene emissions peak during warm,
68 sunnier months of the growing season (MAR-OCT) (Opacka *et al.* 2021). Isoprene has a
69 chemical lifetime of approximately one hour via oxidation by the hydroxyl radical (OH),
70 producing organic aerosols and oxidation products that contribute to ozone (O₃) formation
71 (Carlton *et al.* 2009). Biogenic isoprene emissions affect atmospheric composition and climate,
72 and in turn depend on environmental factors including light, temperature, photosynthetically
73 active radiation (PAR), leaf area index (LAI), water stress, ambient O₃, and CO₂ concentrations.
74 Thus, the response of isoprene emissions to weather extremes and changing climates is highly
75 uncertain.
76

77 Drought is a common abiotic stress to terrestrial ecosystems characterized by low soil
78 moisture, usually associated with high temperature and low precipitation. However, even boreal
79 forests undergo winter drought due to frozen soils. Recent work has shown a strong correlation
80 between drought severity and fine-mode aerosols in the U.S. and estimated that regions
81 undergoing severe drought see up to 17% surface enhancement of aerosols during the growing
82 season (Wang *et al.* 2017). This suggests a strong perturbation of drought to atmospheric
83 aerosols, likely caused by changing BVOC emissions due to drought stress. Limited field and lab
84 measurements have shown that during drought, isoprene has a unique emission response where

85 initial increase in temperature causes an increase in emission, but prolonged or severe drought
86 causes a decrease of emissions due to the shutdown of physiological processes (Potosnak *et al.*
87 2014). This behavior is not reproduced by commonly used BVOC emission models such as the
88 Model of Emissions of Gases and Aerosols from Nature Version 2.1 (MEGAN2.1), which has a
89 simple drought algorithm which is often not used due to the unavailability of the required driving
90 variables in chemistry climate models (CCMs), and the Biogenic Emission Inventory System
91 (BEIS), which does not include a drought algorithm as an option.

92
93 Isoprene flux observations at the Missouri Ozarks (MOFLUX) Ameriflux site in Missouri (SI
94 Fig. S1) recorded a moderate drought in summer 2011 (Potosnak *et al.* 2014) and a particularly
95 severe drought event in summer 2012 (Seco *et al.* 2015). To the best of our knowledge, these are
96 the only in situ isoprene flux measurements capturing a drought anywhere. Using the MOFLUX
97 observations, Jiang *et al.* (2018) developed an isoprene drought stress activity factor for
98 MEGAN3 (Model of Emissions of Gases and Aerosols from Nature Version 3) designed to
99 reduce emissions of isoprene during drought. The previous MEGAN2.1 isoprene drought
100 parameterization utilized soil moisture and soil wilting point threshold to include impacts of
101 drought on photosynthetic processes. The MEGAN3 isoprene drought stress activity factor is a
102 more process-based parameterization based on a photosynthetic parameter ($V_{c,max}$) and water
103 stress (β) from the Community Land Model (CLM) as coupled with the CAM-Chem climate
104 model (Jiang *et al.* 2018). $V_{c,max}$ is the maximum carboxylation capacity of a leaf (usually in units
105 of micromole CO₂ per leaf area per time); that is, it is the ability of a plant to convert CO₂ into
106 sugar, and hence determine productivity of carbon substrates for biogenic volatile organic
107 compounds (BVOCs) production when no other conditions are limiting. β is a scaling factor
108 between zero to one, used in CLM to reduce $V_{c,max}$ due to plant water stress. MEGAN3 isoprene
109 drought stress was also incorporated into the CSIRO chemical transport model (C-CTM) with
110 Australian land surface models Mk3.6 Global Climate Model and the Soil-Litter-Iso model with
111 a focus on Australia (Emmerson *et al.* 2019). Both prior modeling studies (Jiang *et al.* 2018;
112 Emmerson *et al.* 2019) only looked at the drought effects on O₃; here we study the combined
113 effect of drought on O₃ and formaldehyde column.

114
115 The accurate simulation of stress-affected emissions of isoprene during extreme hydroclimate
116 events (i.e. drought) is crucial to understanding vegetation-climate-chemistry feedbacks, because
117 isoprene is a precursor to tropospheric O₃ and SOA, both being climate forcers as well as air
118 pollutants. Here we focus on deriving a model-specific tuned isoprene drought stress factor that
119 is coupled into the existing MEGAN2.1 framework in NASA GISS ModelE, an Earth System
120 Model, to model the effect of drought on isoprene emissions and their effect on atmospheric
121 composition. The model-specific tuning is required due to different land system models
122 parameterizing key variables of $V_{c,max}$ and β in different ways with varying distributions. The
123 model's drought effects will be extensively evaluated over the US, due to the availability of
124 observational evidence during drought (Wang *et al.* 2017). While the MOFLUX data are the only

125 available measurements of isoprene emissions during drought, formaldehyde (HCHO), the high
126 yield oxidation product of isoprene, can be used as a proxy for isoprene emissions (Zhu *et al.*
127 2016). **Section 2** describes the modelling approaches used to represent drought impacts on
128 isoprene emissions. **Section 3** describes the comparison of modeled isoprene emissions to
129 observations at the MOFLUX site during drought along with necessity of building a model
130 specific isoprene drought stress parameterization. **Section 4** details the comparisons between
131 simulation with model specific tuned isoprene drought stress (DroughtStress_ModelE) and
132 observational O₃, PM_{2.5} (particulate matter ≤ 2.5 μm), and tropospheric formaldehyde columns
133 (ΩHCHO) over North America.

134

135 **2. Methods and Data**

136 **2.1. The biogenic emission model MEGAN**

137 MEGAN is a widely used BVOC emissions model that is implemented in many CCMs. Here
138 we describe briefly MEGAN2.1 as implemented in ModelE. MEGAN2.1 calculates the net
139 primary emissions for 20 compound classes, which are speciated into over 150 species such as
140 isoprene, monoterpenes, etc. (Guenther *et al.* 2012). The emissions rate (μg grid cell⁻¹ h⁻¹) of
141 each compound into the above canopy atmosphere from a model grid cell is calculated:

142

$$143 \text{Emission} = EF \times y \times S \quad (1)$$

144

145 where EF (μg m⁻² h⁻¹) is emission factor per compound, y is the dimensionless emission activity
146 factor that accounts for emission response to phenological and meteorological conditions, and S
147 is the grid cell area (m²).

148

149 The emission activity factor y for each compound is calculated following the MEGAN2.1
150 parameterization (Guenther *et al.* 2006; Guenther *et al.* 2012; Henrot *et al.* 2017).

151

$$152 y = y_{CE} \times y_A \times y_d \times y_{CO_2} \quad (2)$$

153

154 Where y_{CE} is the canopy environment coefficient, assigned a value of one for standard
155 conditions, and it takes into account variations associated with LAI (m² m⁻²), photosynthetic
156 photon flux density (PPFD) (μmol of photons in 400-700 nm range m⁻² s⁻¹), and temperature (K).
157 y_A is the leaf age emission activity factor, parameterization of which is based on coefficients of
158 the decomposition of the canopy into new, growing, mature, and senescing leaves for current and
159 previous months' LAI (Guenther *et al.* 2006; Guenther *et al.* 2012). y_d is the isoprene drought
160 stress activity factor and y_{CO_2} is the isoprene emission activity factor associated with CO₂
161 inhibition (for all other compounds y_d and $y_{CO_2} = 1$) (Heald *et al.* 2009). The biogenic emission
162 module implemented in ModelE follows the ECHAM6-HAMMOZ online MEGAN2.1
163 implementation (Henrot *et al.* 2017) in a CCM. Within ModelE the MEGAN2.1 module maps
164 the 16 plant functional types (PFTs) from Ent TBM (Terrestrial Biosphere Model) (Kim *et al.*
165 2015) into 16 MEGAN PFTs, and contains 13 chemical compound classes. ModelE uses a
166 modified MEGAN2.1 following (Henrot *et al.* 2017) to provide a framework to simulate

167 isoprene emissions, and uses prescribed emissions factors per PFT to simulate emissions per
 168 compound class.

169
 170 In Henrot *et al.* (2017) to avoid using a detailed canopy environment model calculating light
 171 and temperature at each canopy depth, the Parameterized Canopy Environmental Emission
 172 Activity (PCEEA) approach from Guenther *et al.* (2006) is used to replace y_{CE} with a
 173 parameterized canopy environment activity factor ($y_{LAI} \times y_P \times y_T$). With this approach the light
 174 dependent and light independent factors are multiplied by y_{LAI} not LAI so they are not directly
 175 proportional to LAI. This approach allows for calculation of light dependent emissions following
 176 isoprene emission response to temperature, where its assumed the light dependent factor (LDF)
 177 equals one for isoprene and light independent emissions follow the monoterpene exponential
 178 temperature response. Please see Guenther *et al.* (2006); Guenther *et al.* (2012); Henrot *et al.*
 179 (2017) for activity factor parameterizations. At any given time step in ModelE, the emissions
 180 formula for a compound class (c) and PFT (i), in units of $\text{kg m}^{-2} \text{s}^{-1}$ is given by:

$$181 \text{Emission}_{i,c} = (1 \times 10^{-9} / 3600) \times (EF_{i,c} \times PFTboxf_i) \times y_{LAI} \times y_A \times y_d \times y_{CO_2} \times ((1 -$$

$$182 LDF) \times y_{TLI} + LDF \times y_P \times y_{TLD}) \times SF_c \times MWC_c \quad (3)$$

184
 185 where $EF_{i,c}$ is the emissions factor ($\mu\text{g m}^{-2} \text{hr}^{-1}$) for a given PFT and compound class, $PFTboxf_i$ is
 186 the fraction of the grid cell (ranging from zero to one) covered by PFT i , and SF_c is a linear scale
 187 factor for compound class c . The activity factors, y , listed in Equation (3) are unitless and
 188 account for the emissions response to leaf area index (LAI), aging (A), drought (d), CO_2 (CO_2),
 189 and PPFD (P). The LDF, weights the contributions from light independent (y_{TLI}) and light
 190 dependent (y_{TLD}) emissions response to temperature. MWC_c stands for a molecular weight
 191 conversion to remove non-carbon mass, if appropriate. ($1 \times 10^{-9} / 3600$): the numerator converts
 192 units from $\mu\text{g}/\text{m}^2/\text{hr}$ to $\text{kg}/\text{m}^2/\text{s}$ and the denominator is the timestep conversion for seconds in an
 193 hour. Note that although the drought activity factor y_d is present in ModelE, it is set to equal one
 194 in all cases prior to this work, meaning no drought effects on BVOC emissions in the model.

195
 196 For example, the emission formula for the compound class of isoprene in ModelE for
 197 PFT i is as follows (where $LDF=1$):

$$198 \text{Isoprene}_i = (1 \times 10^{-9} / 3600) \times (EF_{i,isoprene} \times PFTboxf_i) \times y_{LAI} \times y_A \times y_d \times y_{CO_2} \times (y_P \times y_{TLD}) \times$$

$$199 SF_{isoprene} \times (60.05 / 68.12) \quad (4)$$

202 2.2 MEGAN2.1 Isoprene Drought Stress Emission Algorithm

203 Guenther *et al.* (2006) introduced isoprene drought stress as a soil moisture dependent
 204 algorithm called y_{SM} . This isoprene drought stress activity factor relied upon soil moisture and
 205 wilting point to apply drought stress to isoprene emissions. The algorithm for soil moisture
 206 isoprene drought stress is as follows:

207

208 $y_{SM} = 1$ when $\theta > \theta_1$ (5a)

209 $y_{SM} = \frac{\theta - \theta_w}{\Delta\theta_1}$ when $\theta_w < \theta < \theta_1$ (5b)

210 $y_{SM} = 0$ when $\theta < \theta_w$ (5c)

211

212 where θ is soil moisture (volumetric water content $\text{m}^3 \text{m}^{-3}$), θ_w is the point beyond which plants

213 cannot extract water from soil, known as the wilting point, $\text{m}^3 \text{m}^{-3}$, $\Delta\theta_1$ ($=0.06$ in Guenther et al.

214 2006 and $=0.04$ in Guenther et al. 2012) is an empirical parameter, and θ_1 is defined as $\theta_w +$

215 $\Delta\theta_1$. Soil moisture and wilting point are not widely available parameters in models, and y_{SM} was

216 not widely adopted to represent isoprene drought stress as studies showed substantial uncertainty

217 associated with soil moisture predicted response of isoprene emission to water stress and in

218 selection of wilting point values (Müller *et al.* 2008; Tawfik *et al.* 2012; Sindelarova *et al.* 2014;

219 Huang *et al.* 2015; Jiang *et al.* 2018). There also exist challenges associated with validating soil

220 moisture datasets due to the limited spatial coverage of in-situ root-zone measurements in the

221 contiguous United States (Ochsner *et al.* 2013). A study found that the accurate simulation of

222 soil moisture in land surface models was highly model-dependent, due to the differing horizontal

223 and vertical spatial resolution of such models at large scales (Koster *et al.* 2009). Potosnak *et al.*

224 (2014) determined that the selection of different wilting point values greatly impacted the

225 drought impacts on biogenic isoprene emission. With these associated challenges, it was rare to

226 find isoprene drought stress implemented in CCMs, thus a new isoprene drought activity factor

227 needed to be developed that could be easily incorporated into a variety of models that had a land

228 surface model (LSM) or terrestrial biosphere model (TBM).

229

230 **2.3 MEGAN3 Isoprene Drought Stress Emission Algorithm**

231 Jiang *et al.* (2018) developed a new isoprene drought stress activity factor in MEGAN3 that

232 focuses on photosynthetic carboxylation capacity and water stress to model reductions of

233 vegetative isoprene during drought. Vegetation responds to high water stress by undergoing

234 physiological, morphological, and biochemical changes (Seleiman *et al.* 2021). During high

235 water stress plants experience leaf area reduction and loss of leaves, decreasing photosynthetic

236 rate due to stomatal closure, decreasing stomatal conductance, transpiration, and evaporative

237 cooling. There is also during drought decreasing rubisco efficiency, which is the enzyme used for

238 carbon fixation of atmospheric CO_2 into useable sugar molecules during photosynthesis

239 (Seleiman *et al.* 2021). These are just a few of the ways vegetation respond to water stress, which

240 impact isoprene emissions. The algorithm was developed using isoprene flux observations during

241 the severe drought of the summer of 2012 and less severe drought of 2011 (Potosnak *et al.* 2014;

242 Seco *et al.* 2015) at MOFLUX. The MOFLUX site is located in the University of Missouri

243 Baskett Wildlife Research area in central Missouri which is known as the isoprene volcano

244 (Wells *et al.* 2020). The MOFLUX site is comprised primarily of deciduous broadleaf trees,

245 primarily oaks, known to emit high quantities of isoprene. All meteorological data from the site

246 comes from the Ameriflux website (<https://ameriflux.lbl.gov/sites/siteinfo/US-MOz#overview>).

247

248 We refer to the original MEGAN3 drought stress developed by Jiang *et al.* (2018) to be
 249 **DroughtStress_MEGAN3_Jiang**, and the corresponding parameterization for isoprene activity
 250 factor during drought where (y_d) is a function of PFT and where the values of $V_{c,max}$ and β are
 251 specified by PFT is:

$$252 \quad y_d = 1, \text{ when } \beta \geq 0.6 \quad (6a)$$

$$253 \quad y_d = \frac{(V_{c,max} \times \beta)}{\alpha}, \text{ when } \beta < 0.6, \alpha = 37 \quad (6b)$$

$$254 \quad 0 \leq y_d \leq 1 \quad (6c)$$

$$255 \quad Isoprene_i = (1 \times 10^{-9} / 3600) \times (EF_{i,isoprene} \times PFTboxf_i) \times y_{LAI} \times y_A \times y_d \times y_{CO_2} \times (y_P \times y_{TLD}) \times$$

$$256 \quad SF_{isoprene} \quad (7)$$

257 The drought stress activity factor, y_d , in **DroughtStress_MEGAN3_Jiang** was originally
 258 developed using the Community Land Model Version 4.5 (CLM4.5) (Jiang *et al.* 2018). The
 259 photosynthetic parameter used is $V_{c,max}$, which is the maximum rate of leaf-level carboxylation.
 260 In ModelE, $V_{c,max}$ is scaled with an enzymatic kinetics response to temperature, and drought
 261 stress reduces leaf stomatal conductance, thereby reducing photosynthetic activity through CO₂
 262 diffusion limitation rather than by reduction of $V_{c,max}$. In CLM4.5, $V_{c,max}$ is a function of nitrogen
 263 (Jiang *et al.* 2018). Water stress in CLM4.5 is based on soil texture (Clapp and Hornberger
 264 1978), and it is a function of soil water potential of each soil layer, wilting factor, and PFT root
 265 distribution. Water stress (β) ranges from zero when a plant is completely stressed to one when a
 266 plant is not undergoing stress. In CLM4.5, $V_{c,max}$ is scaled online by β before being applied into
 267 the isoprene drought activity parameterization, thus this scaling step is not reflected in the
 268 equations shown by Jiang *et al.* (2018). Since ModelE does not scale $V_{c,max}$ by β (instead,
 269 ModelE scales leaf stomatal conductance by β), to reproduce the original scheme by Jiang *et al.*
 270 (2018) as much as possible in ModelE, we scaled $V_{c,max}$ with β inside the equation of isoprene
 271 drought activity factor as in Eq. (6b). y_d as defined in Eq. (6) is then applied in ModelE as an
 272 activity factor into the MEGAN2.1 isoprene emissions equation per every plant functional type
 273 (PFT) and the modeling results from this simulation are referred to as
 274 **DroughtStress_MEGAN3_Jiang**. The y_d ranges from zero to one and is designed to reduce
 275 isoprene emissions during severe and prolonged drought.

276 2.4 NASA GISS ModelE Climate Chemistry Model

277 NASA GISS ModelE2.1 is an Earth System Model (ESM) with a horizontal and vertical
 278 resolution of 2° degrees in latitude and 2.5° degrees in longitude with 40 vertical layers from the
 279 surface to 0.1 hPa (Kelley *et al.* 2020). The climate model is configured in CMIP6 (Coupled
 280 Model Intercomparison Project Phase 6) configuration (Miller *et al.* 2021) with fully coupled
 281 atmospheric composition with interactive gas-phase chemistry. The model described here is
 282 driven by historical Atmospheric Model Intercomparison Project simulations (AMIP), using
 283 prescribed ocean temperature and sea ice datasets. There are two aerosol schemes to choose
 284

288 from: MATRIX (“Multiconfiguration Aerosol TRacker of mIXing state”) (Bauer *et al.* 2008) a
289 microphysical aerosol scheme and OMA (One-Moment Aerosol) mass-based aerosol scheme
290 (Koch *et al.* 2006; Miller *et al.* 2006; Bauer *et al.* 2007; Tsigaridis *et al.* 2013; Bauer *et al.* 2020).
291 Here we use the OMA scheme, due to its better representation of secondary organic aerosol
292 chemistry (Tsigaridis *et al.* 2013). SOA is calculated using the CBM4 chemical mechanism to
293 describe the gas phase tropospheric chemistry together with all main aerosol components
294 including SOA formation and nitrate, and is calculated using four tracers in the model. Isoprene
295 (VOCs) contribute to the formation of SOA. OMA has 34 tracers for the representation of
296 aerosols that are externally mixed, except for mineral dust that can be coated (Bauer *et al.* 2007),
297 and has prescribed constant size distribution (Bauer *et al.* 2020). OMA aerosol schemes are
298 coupled to the stratospheric and tropospheric chemistry scheme (Shindell *et al.* 2013) which
299 includes inorganic chemistry of O_x, NO_x, HO_x, CO, and organic chemistry of CH₄ and higher
300 hydrocarbons, with explicit treatment of secondary OA (organic aerosol), and the stratospheric
301 chemistry scheme which includes chlorine and bromine chemistry together with polar
302 stratospheric clouds. O₃ and aerosols impact climate via coupling to the radiation scheme, and
303 aerosols serve as cloud condensation nuclei (CCN) for cloud activation. The model includes the
304 first indirect effect. Sea salt, dimethyl sulfide (DMS), and biogenic dust emission fluxes are
305 calculated interactively, while anthropogenic dust is not represented in ModelE2.1. Other
306 anthropogenic fluxes are from the Community Emissions Data System Inventory (CEDS)
307 (Hoesly *et al.* 2018) and biomass burning is from GFED4s (Global Fire Emissions Database with
308 small fires) inventory (van Marle *et al.* 2017) for 1850-2014.

309
310 Vegetation activity in ModelE is simulated with a dynamic global vegetation model, the Ent
311 Terrestrial Biosphere Model (Ent TBM) (Kim *et al.* 2015). In standard ModelE experiments, the
312 Ent TBM prescribes satellite-derived vegetation canopy structure (plant functional type, canopy
313 height, monthly leaf area index) (Ito *et al.* 2020) as boundary conditions for coupling the
314 biophysics of canopy radiative transfer, photosynthesis, vegetation and soil respiration, and
315 transpiration with the land surface model and atmospheric model. These processes provide
316 surface fluxes of CO₂ and water vapor, and surface albedo is specified by cover type and season.
317 ModelE uses the MEGAN2.1 BVOC emissions model to simulate interactive biogenic emissions
318 from vegetation (Guenther *et al.* 2006; Guenther *et al.* 2012). Ent TBM water stress is calculated
319 as a scaling factor between zero and one as a function of relative extractable water (REW) for the
320 given soil texture and PFT-dependent levels of REW for onset of stress and wilting (Kim *et al.*
321 2015); this scaling has been updated since Kim *et al.* (2015) to be a function of the water stress
322 factor of only the wettest soil layer in the PFT’s root zone. Ent TBM uses a leaf-level model of
323 coupled Farquhar-von Caemmerer photosynthesis/Ball-Berry stomatal conductance (Farquhar
324 and von Caemmerer 1982; Ball and Berry 1985). The model calculates an unstressed leaf
325 photosynthesis rate and stomatal conductance, then applies its water stress scaling factor to scale
326 down leaf stomatal conductance, to emulate how hormonal signaling by roots under water stress
327 induces stomatal closure. Since there is a coupling of transpiration and CO₂ uptake through

328 stomatal conductance, water stress thereby also reduces photosynthesis rate through the
329 limitation on CO₂ diffusion into the leaf; this is different from CLM4.5's approach, which
330 instead reduces $V_{c,max}$. Canopy radiative transfer in the Ent TBM scales leaf processes to the
331 canopy scale by calculating the vertical layering of incident photosynthetically active radiation
332 on sunlit versus shaded leaves. The different PFTs in Ent TBM have different critical soil
333 moisture values for the onset of stress (when stomatal closure begins in response to drying soils)
334 and their wilting point (when the plant is unable to withdraw moisture from the soil and complete
335 stomatal closure occurs). It should be noted that the GISS land surface model is wetter than
336 observed soil moisture (Kim *et al.* 2015). $V_{c,max}$ is a function of a Q₁₀ temperature function in
337 ModelE. Since nitrogen dynamics are not represented yet in the Ent TBM, leaf nitrogen is fixed
338 and therefore $V_{c,max}$ is not dynamic with nitrogen as in CLM4.5. The Q₁₀ coefficient is often used
339 to predict the impact of temperature increases on the rate of metabolic change (Rasmusson *et al.*
340 2019).

341
342 To emulate the MEGAN/CLM representation of drought stress, in this study, in the Ent TBM
343 leaf model, we applied a reduction in $V_{c,max}$ with water stress as shown in Eq. (6b). It is important
344 to note that the reduction of $V_{c,max}$ with water stress in Eq. (6b), is not used outside the isoprene
345 drought stress parameterization, so the $V_{c,max}$ reduction is not applied to the calculation of
346 photosynthetic CO₂ uptake; this avoids applying another secondary indirect scaling to
347 conductance, since the Ent TBM already applies its water stress factor to reduce stomatal
348 conductance.

349
350 For this study, ModelE2.1 was configured with a transient atmosphere and ocean using a
351 prescribed sea surface temperature (SST) and sea ice (SSI) according to observations. The
352 transient simulations contain continuously-varying greenhouse gases in order to represent a
353 realistic mode in present day. To facilitate direct comparison with atmospheric composition
354 observations as in this study, meteorology is nudged to the National Centers for Environmental
355 Prediction (NCEP) reanalysis winds. Four transient ModelE simulations were run for the period
356 of 2003-2013 with a three-year spin-up using MEGAN2.1 with varying configurations for
357 isoprene drought stress to be described below. The authors found that the default MEGAN
358 implementation in ModelE2.1 underestimates isoprene and monoterpene emissions, thus
359 appropriate scaling factors (SF_c) were applied to match literature for global annual emission
360 estimates, 1.8 for isoprene and 3 for monoterpenes to match literature estimates of around ~500
361 Tg C of isoprene and ~130 Tg C of monoterpenes (Arneth *et al.* 2008; Guenther *et al.* 2012).

362 363 **2.5 Observations of Isoprene Emissions at MOFLUX during Drought of 2011-2012**

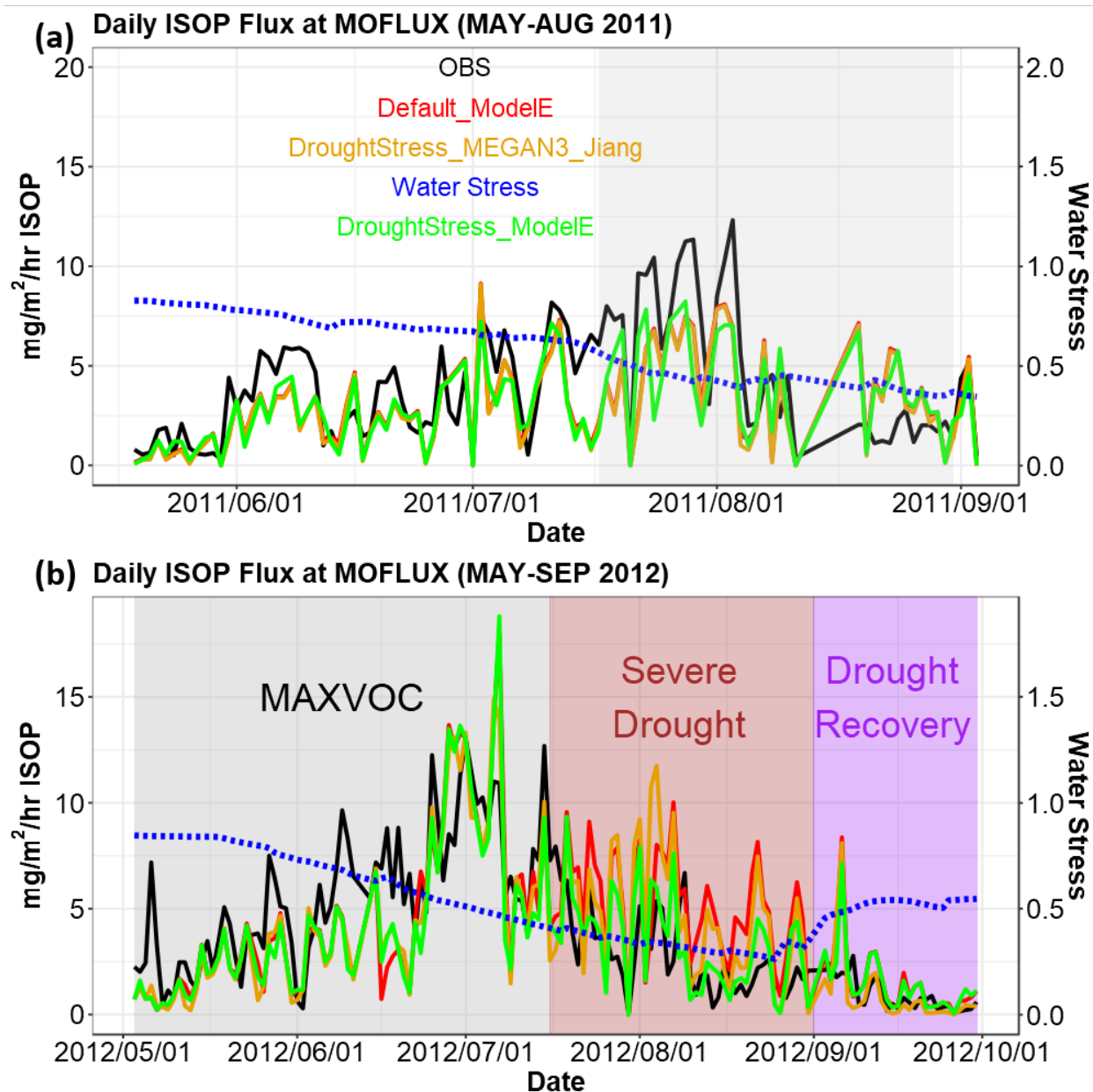
364 The MOFLUX site located at 38.7441°N, -92.2000°W (latitude, longitude) is comprised
365 mostly of deciduous broadleaf forests dominated by oak-hickory forest and the climate is
366 classified as humid subtropical with no dry season and hot summers. The site experienced a mild
367 drought in the mid to late summer of 2011 and an extreme to exceptional drought from the mid

368 to late summer of 2012 when concurrent biogenic isoprene flux measurements were taken. The
369 2011 drought was not as severe as the drought of summer of 2012. The ecosystem response of
370 isoprene has two stages including a mild phase of drought stress where emissions are stimulated
371 by increases in leaf temperature due to reduced stomatal conductance while in the second stage
372 of drought, the more severe phase of drought stress, emissions are suppressed by reduction in
373 substrate availability or isoprene synthase production (Potosnak *et al.* 2014; Seco *et al.* 2015).

374
375 In 2011, the spring was wet but the drought started to appear in June due to lack of rainfall
376 while temperatures broke records and continued through July (Potosnak *et al.* 2014; Jiang *et al.*
377 2018). The U.S. Drought Monitor (USDM) produces color-coded maps indicating drought
378 severity across the U.S. and is produced through a partnership of the National Drought
379 Mitigation Center at the University of Nebraska-Lincoln, the U.S. Department of Agriculture,
380 and the National Ocean and Atmospheric Administration (NOAA). The USDM drought maps
381 have five classifications to indicate drought condition: (D0) indicating abnormally dry, (D1)
382 moderate drought, (D3) extreme drought, and (D4) exceptional drought. However, the USDM
383 did not capture this drought signal from June - July and only showed abnormally dry periods
384 from August 2 - August 16, and never went into extreme (D2) or severe drought stage (D3). This
385 suggests 2011 summer was a useful case only for studying drought response of isoprene during
386 weak drought conditions. The highest observed isoprene fluxes were from July 11 – August 3
387 shown in Fig. 1a. Potosnak *et al.* (2014) reported that from July 14 - August 10 their MEGAN2.1
388 simulations consistently underestimated isoprene emissions during onset of drought and
389 overestimated as drought progressed from August 18 to September 2. From August 3 – August
390 23 there was a total of 65 mm of precipitation, which led to an increase in observed soil
391 moisture. It was suggested that since observed soil moisture increases during the period of
392 drought progression when isoprene is decreasing (August 18 - September 2) relative to the onset
393 of drought (July 14 - August 10), this indicates the response to drought stress during this year is
394 time dependent, and a time-independent algorithm based on soil moisture will not capture the
395 relevant processes during a less severe drought year. It was also noted that MEGAN2.1
396 underpredicts during the cooler months of May-June and underpredicts during the warmer month
397 of July (Potosnak *et al.* 2014), and only overpredicts during small portions of August-September
398 as denoted by a grey box in Fig. 1a. With this pattern of underprediction observed in MEGAN2.1
399 simulations and also seen in Default_ModelE, as well as weak drought conditions as stated
400 above, 2011 is not an ideal year to tune an isoprene drought stress algorithm to target the
401 reduction period caused by drought stress.

402
403 In 2012, there were three unique periods that displayed the development of a severe drought
404 that make it ideal to tune an isoprene drought stress algorithm. Shown in Fig. 1b is the daily
405 averaged isoprene flux broken up into three periods. We define the MAXVOC episode from
406 May 1 - July 16, severe drought period (July 17-August 31) shaded in brown in Fig. 1b, and the
407 drought recovery period (September 1-31). Although Seco *et al.* (2015) defined MAXVOC from

408 June 18 – July 31, they identified July 16 as the transitional stage between MAXVOC episode
409 and severe drought. Thus, our work used July 16 to separate MAXVOC and severe drought
410 periods. The periods of pre-drought (prior to May 31) and mild drought identified by Seco *et al.*
411 (2015) from May 31- June 14 are included in the MAXVOC period, because during this time
412 period a typical seasonal pattern of increasing emissions with increasing temperatures is shown,
413 and there is no indication of decreasing emissions due to drought stress. The mild drought period
414 (May 31- June 14) corresponds to USDM periods of abnormally dry and moderate drought.
415 Isoprene emissions continue to increase during the beginning of summer, which is supported by
416 several studies that show isoprene emissions during the first stages of drought increase even
417 though there is a decrease in CO₂ fixation, which is attributed to drought induced stomatal
418 closure and rising leaf temperature and decreasing transpirational cooling and CO₂ concentration
419 in the leaf (Rosenstiel *et al.* 2003; Pegoraro *et al.* 2004; Potosnak *et al.* 2014; Seco *et al.* 2015).
420 Separating MAXVOC and severe drought period allows for the algorithm development to target
421 the latter severe drought stage where isoprene reduction occurs, while not reducing emissions
422 during the early, and less severe, stages of drought. During the severe drought period, total
423 annual precipitation was the lowest in a decade while soil water content reached its minimum at
424 the end of August when the drought peaked (Jiang *et al.* 2018). During the severe drought there
425 is a marked decrease in isoprene flux shown by the brown shaded box coinciding with lower β
426 values. It is well established that isoprene emissions are linked to high temperatures (Singsaas
427 and Sharkey 2000), and without the contributing factor of drought there should be a rising
428 increase in isoprene emissions in July and August. The severe drought period encompasses
429 periods of severe and extreme drought identified by the USDM. July 3 marks the first week
430 indicated by USDM of severe drought and July 31 marks the first week of extreme drought.
431 During severe drought isoprene production is suppressed by reductions in substrate availability
432 and isoprene synthase transcription (Potosnak *et al.* 2014). Rain events at the end of August led
433 to drought recovery and soil water content started to increase, which is indicated by increasing β
434 values shown in the drought recovery period indicated in purple in Fig. 1b. Overall, 2012 shows
435 a complete development of drought conditions that affect isoprene emissions and will provide
436 useful constraints on the drought stress factor parameterization: a MAXVOC period that
437 encompasses pre- and mild drought periods, a severe drought period (July 17 – August 31), and a
438 drought recovery period (September 1-30). Included in the supplement SI Fig. S8 is distributions
439 of daily averaged isoprene flux split in MAXVOC, severe drought period, and drought recovery
440 period for simulations Default_ModelE and DroughtStress_ModelE compared to observations.



442 Figure 1. Daily isoprene emissions flux at MOFLUX (MAY-AUG 2011 and MAY-SEP 2012) LST timeseries are shown.
 443 Black shows observed isoprene emissions (abbreviated as ISOP), red shows Default_ModelE without isoprene drought
 444 stress, orange shows DroughtStress_MEGAN3_Jiang, and green shows DroughtStress_ModelE with units of $\text{mg/m}^2/\text{hr}$ of
 445 isoprene. (a) Shaded in the grey region from JUL 17 through AUG 31 of 2011, is the period where water stress falls below
 446 0.4 for short periods. (b) Shaded in grey is the MAXVOC period, and shaded in brown is the period of severe/extreme
 447 drought from July 17 through August 2012, and shaded in purple is the drought recovery period.

448

449 2.6 Offline Isoprene Emissions Model

450 An offline model was created based on the isoprene emissions formula Eq. (4) of the
451 MEGAN module contained in ModelE in order to develop the new parametrization in a timely
452 fashion without waiting for online transient simulations to complete. ModelE was first run in a
453 default transient simulation with MEGAN2.1 where no isoprene drought stress was applied,
454 referred to as **Default_ModelE**, from which the MEGAN activity factors and variables required
455 to drive the offline calculation of isoprene emissions were output and archived. Default_ModelE
456 was compared to observed temperature at MOFLUX in SI Fig. S10, S12a as temperature is the
457 main biogenic driver of isoprene (Mishra and Sinha 2020; Jiang *et al.* 2018). Default_ModelE
458 was also compared to sensible heat and latent heat in SI Fig. S11 as the exchange of latent and
459 sensible heat fluxes is one of the most important aspects of land-atmosphere coupling as these
460 energy fluxes are affected by partitioning of net radiation absorbed by the surface, which
461 influence atmospheric dynamics, influence boundary layer structure, cloud development, and
462 rainfall (Gu *et al.* 2016). We verified LAI at the MOFLUX site during 2012 in SI Fig. S12b
463 using the NOAA Climate Data Record AVHRR (Advanced Very High Resolution Radiometer)
464 LAI dataset (Vermote 2019) that we averaged on a monthly scale and regridded from
465 $0.05^\circ \times 0.05^\circ$ to match ModelE's horizontal resolution. Other monthly averaged meteorological
466 variables at MOFLUX during 2012: temperature, LAI, relative humidity, shortwave incoming
467 solar radiation, CO₂ flux, vapor pressure deficit (VPD), and canopy conductance are compared to
468 observed when observations are available in SI Fig. S12. Soil moisture by layer is shown in SI
469 Fig. S14. The offline model was then driven by these outputs at the half hourly timestep to match
470 with the 30-minute timestep in the online calculation of physics and the MEGAN module. The
471 offline model was verified by making sure outputs of isoprene emissions matched the online
472 Default_ModelE simulation. With the verified offline model, different parameterizations of
473 isoprene drought stress could be tested and cross verified with observations at MOFLUX. The
474 offline model is used to derive a model specific α and β threshold (Eq. (6a-6c)) for ModelE in
475 order to create the appropriate parameterization of a model specific isoprene drought stress in
476 ModelE known as **DroughtStress_ModelE**, described in Section 3.3. Since models calculate
477 water stress and $V_{c,max}$ in different ways, the offline model is the necessary step to derive model-
478 specific water stress thresholds to target drought periods and ensure α and β are being applied
479 correctly.

480

481 2.7 ModelE Sensitivity Simulations

482 Four transient global ModelE simulations were configured for the period of 2003-2013 with
483 a three-year spin-up, as described in **Table 1**. A default simulation (Default_ModelE) that set y_a
484 =1 was performed where no isoprene drought stress parameterization was applied. A second
485 simulation named DroughtStress_MEGAN3_Jiang was performed as a sensitivity test to
486 determine the efficacy of the DroughtStress_MEGAN3_Jiang algorithm Eq. (6a-6c), which is
487 not tuned specifically for ModelE, and was originally developed by Jiang *et al.* (2018) as a non-
488 model specific tuned isoprene drought stress formula to be used widely in models. A third
489 simulation was performed with the offline derived ModelE tuned isoprene drought stress

490 parameterization to best fit MOFLUX observations (MOFLUX_DroughtStress) using Eq. (8a-
 491 8c) to be described in Section 3.2. A fourth simulation called DroughtStress_ModelE was
 492 performed using a subset of parameters derived from MOFLUX_DroughtStress but a different
 493 drought activation method in Section 3.3 using Eq. (10a-10b).

494
 495

Table 1. ModelE Online Transient Simulation Descriptions

Simulation Name	Drought Stress	Isoprene Emission Eqn.	β Threshold	α
1) Default_ModelE	NO	Eq. (4)	N/A	N/A
2) DroughtStress_MEGAN3_Jiang	YES Eq. (6a-6c)	Eq. (7)	$\beta < 0.6$	37
3) MOFLUX_DroughtStress	YES Eq. (8a-8c)	Eq. (9)	$0.25 < \beta < 0.40$	100
4) DroughtStress_ModelE	YES Eq. (10a-10b)	Eq. (9)	$\beta < 4^{\text{th}}$ percentile	100

496

3. Development of Model specific Drought Stress Parameterization

497

3.1. MOFLUX Single Site Observational Comparison to Model

498

499 Shown in Fig. 1a is the 2011 timeseries of biogenic isoprene flux at the MOFLUX site of two
 500 online simulations Default_ModelE (red) and DroughtStress_MEGAN3_Jiang (orange)
 501 compared to observations (black). In 2011, Default_ModelE tended to underestimate isoprene
 502 flux during onset of drought (July 14 - August 10) and had minor periods of overestimation
 503 during drought progression (August 18 – September 2) which was also seen by MEGAN2.1
 504 simulations of Potosnak *et al.* (2014). DroughtStress_MEGAN3_Jiang simulation applied
 505 isoprene drought stress from mid-July through September when β fell below the 0.6 threshold
 506 identified by Jiang *et al.* (2018). In the DroughtStress_MEGAN3_Jiang simulation it is shown
 507 that during the drought progression stage, DroughtStress_MEGAN3_Jiang isoprene is reduced
 508 compared to Default_ModelE, but reductions are not strong enough to align with lower observed
 509 values for a majority of this period. The timeseries shows that there is little deviation between
 510 the Default_ModelE and DroughtStress_MEGAN3_Jiang during the 2011 mild drought.

511

512 Shown in Fig. 1b is the 2012 timeseries of biogenic isoprene flux at the MOFLUX site of two
 513 online simulations Default_ModelE and DroughtStress_MEGAN3_Jiang compared to
 514 observations, with β (blue). Default_ModelE typically underestimates isoprene flux during the
 515 MAXVOC period, overestimates during the severe drought period, and reproduces the drought
 516 recovery period sufficiently except for September 6 where the model greatly overestimates
 517 leading to a peak not matched by observations. During the severe drought period the
 518 Default_ModelE mean bias (MB) $\cong 2.20 \text{ mg/m}^2/\text{hr}$ and the normalized mean bias (NMB) \cong
 519 76.10%. β daily average values fell below the 0.60 threshold on June 20 and continued below the
 520 threshold through September 3. With the β falling below 0.60, the

521 DroughtStress_MEGAN3_Jiang simulation starts reducing isoprene during the MAXVOC
522 period and continues to reduce through the drought recovery period. This leads to compounding
523 the underestimation during the MAXVOC period, small corrections to overestimation during
524 severe drought but missing the peak overestimations, and too large of reductions of isoprene
525 during drought recovery period. During the severe drought period the MB of
526 DroughtStress_MEGAN3_Jiang was $\cong 1.61$ mg/m²/hr and the NMB was $\cong 55.81\%$.
527 DroughtStress_MEGAN3_Jiang thus decreased the overestimation by $\sim 20.29\%$ during the
528 severe drought period. The timeseries comparison for 2012 indicates the parameters in the Jiang
529 et al. parameterization resulted in only minor improvements in ModelE for the severe drought
530 period, because they were tuned for CLM4.5. The DroughtStress_MEGAN3_Jiang simulation
531 shows that the α and β need to be tuned on a model-by-model basis. Based on these minor
532 improvements, and the differences in how $V_{c,max}$ and β are calculated in CLM4.5 versus Ent
533 TBM, it was clear a model tuned parameterization could be used to further improve the
534 relationship of simulated isoprene emissions during drought.

535

536 **3.2 Site Tuned MOFLUX_DroughtStress Parameterization**

537 Using the offline isoprene emissions model (Section 2.6) driven by catalogued variables from
538 each time step of the **Default_ModelE** simulation and the MOFLUX biogenic isoprene flux
539 measurements for 2012, we describe here how a water stress threshold to target severe/extreme
540 drought periods and a model appropriate empirical variable (α) were derived to create the
541 isoprene drought stress parameterization based upon the framework of Eq. (6a-6c), called
542 **MOFLUX_DroughtStress**. MOFLUX_DroughtStress was developed to target the 2012 severe
543 drought period shown in Fig. 1b as this period is when the model overestimates despite
544 observations showing decreasing emissions during drought. The water stress threshold range
545 targeting the severe drought period determines when the isoprene drought stress is applied and it
546 is bounded to exclude the period of drought recovery and the onset of drought when isoprene
547 emissions are still increasing. The range of β specific to ModelE is 0.25 to 0.40 during the severe
548 drought period, which differs from the CLM4.5 threshold of 0.60 as it is a model specific
549 parameterization. Isoprene drought stress in MOFLUX_DroughtStress is thus applied only when
550 $\beta < 0.40$, and at all other β values $y_d = 1$.

551

552 To find the empirical variable, α , an offline sensitivity analysis was conducted using the
553 offline isoprene emissions model with 0.25 to 0.40 as the β threshold to activate isoprene
554 drought stress. The PFT weighted value of $V_{c,max}$ and β were used to calculate the y_d in the
555 offline isoprene emissions model. A range of α values from 60 to 160 were tested in Eq. (8a-8c)
556 to find y_d . y_d dependence on the value of α was fed into Eq. (9) to output offline isoprene
557 emissions. The offline modeled emissions from Eq. (9) were evaluated against observed isoprene
558 fluxes at MOFLUX, and it was determined that $\alpha = 100$ gave the best fit and strongest
559 relationship between the offline modeled emissions and measured isoprene at MOFLUX. $\alpha = 100$
560 had the lowest NMB closest to zero during the severe drought period, and the most improved

561 slope, y-intercept, and correlation coefficient during the summer of 2012. The α variable, though
 562 empirically derived, is strongly related to the model specific $V_{c,max}$ which is why our alpha differs
 563 from DroughtStress_MEGAN3_Jiang, where $\alpha = 37$. Based on the offline emissions comparisons
 564 to observed it was determined that **MOFLUX_DroughtStress** is defined as follows:

$$565 \quad y_d = 1 \quad (\beta \geq 0.4) \quad (8a)$$

$$567 \quad y_d = \frac{(v_{c,max} \times \beta)}{\alpha} \quad (0.25 < \beta < 0.40) \quad \text{where } \alpha = 100 \quad (8b)$$

$$568 \quad y_d = 1 \quad (\beta \leq 0.25) \quad (8c)$$

$$570 \quad Isoprene_i = (1 \times 10^{-9} / 3600) \times (EF_{i,isoprene} \times PFT_{boxfi}) \times y_{LAI} \times y_A \times y_d \times y_{CO_2} \times (y_P \times y_{TLD}) \times$$

$$571 \quad SF_{isoprene} \quad (9)$$

572
 573 Where y_d uses the area weighted average over PFTs of $v_{c,max}$ and β in Eq. (8a-c), and thus y_d in
 574 Eq. (9) is not a function of PFT, which differs from DroughtStress_MEGAN3_Jiang Eq. (7)
 575 where y_d is a function of PFT.

576
 577 MOFLUX_DroughtStress simulation with isoprene drought stress applied Eq. (8a-8c) is
 578 found to reduce the MB at the MOFLUX site to $\cong 0.04$ mg/m²/hr during the 2012 severe drought
 579 period, indicating the parameterization is able to correct the model overestimation of isoprene
 580 emissions. Scatterplots and timeseries of the simulation MOFLUX_DroughtStress during MAY-
 581 SEP 2012 are included in SI Fig. S2. The NMB decreased to $\cong 1.53\%$, indicating a $\sim 74.57\%$
 582 reduction compared to Default_ModelE. Large improvements were not expected for 2011 as this
 583 algorithm was designed to target severe/extreme drought. Despite the better agreement between
 584 measured and modeled fluxes in MOFLUX_DroughtStress at the MOFLUX site, the regional
 585 analysis described below determined that water stress values are region specific and a new
 586 approach was needed in order to make the algorithm applicable for other regions in the global
 587 model.

588 **3.3 New Percentile Threshold Isoprene Drought Stress Parameterization**

589 After implementing MOFLUX_DroughtStress in ModelE, we found for JUN-AUG 2011
 590 isoprene emissions reductions for the southeastern (SE) U.S. defined as (96-75°W, 25-38°N) of
 591 approximately -3.5%, -7.2%, -5.7% respectively. These regional reductions were smaller than
 592 expected as the SEUS 2011 was a spatially extensive severe drought over a largely forested and
 593 vegetated region. The US Drought Monitor (USDM) reported that the southeast area in moderate
 594 to exceptional drought for JUN-AUG 2011 was 63%, 61%, and 55% respectively. Other studies
 595 for other regions of the world have reported during severe drought that reductions in isoprene
 596 vary by region and have a large uncertainty. For example, Huang et al. (2015) reported using
 597 different soil moisture products that resulted in isoprene reductions of 12-70% for Texas. Others
 598 showed reductions up to a maximum of 17% (Jiang et al. 2018; Wang et al. 2021). The reason
 599 why MOFLUX_DroughtStress falls on the lowest end of reported isoprene reductions for the
 600

601 regional analysis is probably because drought stress activation was calibrated to water stress
602 ranges at a single site. As water stress is expected to vary regionally, a new regional method was
603 needed in order to simulate drought stress effects globally.

604

605 A new parameterization was designed to not only work at MOFLUX since this is the site
606 used for validation, but capture isoprene drought signals for other regions. To do so, we first
607 simulated daily averaged water stress during the growing season for ten years (2003-2012) at
608 MOFLUX, a total of 2450 days. It was determined that water stress was less than the 0.4
609 threshold for 102 days, a percentage of ~ 4.16%. For simplicity, we rounded the percentage to
610 4%. The new approach then relied upon finding the 4th percentile water stress value across ten
611 years of daily water stress per grid and for each individual month in order to build a
612 parameterization that would capture regional and seasonal variability in water stress in ModelE.
613 This new drought stress parameterization is known as DroughtStress_ModelE and uses the same
614 alpha ($\alpha=100$) as MOFLUX_DroughtStress and is applied as weighted average per PFT. What
615 makes this different from the previous approach, MOFLUX_DroughtStress, is that the water
616 stress threshold used to apply drought stress is based on the model's unique lowest 4th percentile
617 of water stress on a grid-by-grid basis and is not based on the absolute values of water stress at a
618 single site (i.e., MOFLUX) and is a statistical tuning method. The 4th percentile of daily water
619 stress was used as the trigger for drought stress activation. The parameterization for

620 **DroughtStress_ModelE** is Eq. (10a-10b):

621

$$622 \quad y_d = 1 \quad \text{when } (\beta \geq 4^{\text{th}} \text{ percentile}) \quad (10a)$$

$$623 \quad y_d = \frac{(v_{c,max} \times \beta)}{\alpha} \quad \text{when } (\beta < 4^{\text{th}} \text{ percentile}), \text{ where } \alpha=100 \quad (10b)$$

624

625 A global transient simulation was run from (2003-2013) applying Eq. (10a-10b) globally,
626 called DroughtStress_ModelE in order to determine the effects of the isoprene drought stress
627 parameterization and to see if it captures the signal of the 2011 SE drought.

628 DroughtStress_ModelE for JJA 2011 showed isoprene emissions percent reductions for the SE of
629 approximately -9.6%, -5.9%, and -12.7% respectively. These reported reductions are a factor of
630 two greater than MOFLUX_DroughtStress for the same period, and are in the mid-range of
631 reported isoprene reductions during drought. A complete timeseries of isoprene emissions at
632 MOFLUX for all four simulations as described by **Table 1** is shown in SI Fig. S2a-b for 2011
633 and 2012.

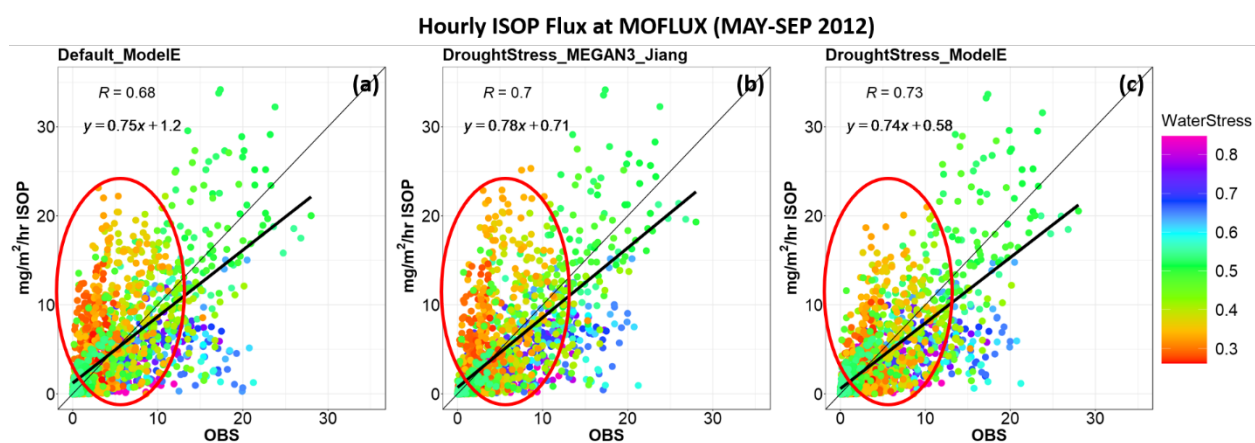
634

635 **3.4 DroughtStress_ModelE Evaluation at MOFLUX**

636 During 2011 at the MOFLUX site, there were only small differences between
637 Default_ModelE and DroughtStress_ModelE. The scatterplots of isoprene emissions at the
638 MOFLUX site for the summer of 2011 show the hourly correlation coefficient between modeled
639 and observed isoprene fluxes showed minor improvement from 0.77 to 0.78, with minor changes
640 in slope and y-intercept (SI Fig. S3a,c). The diurnal cycles for 2011 included in (SI Fig. S4a)

641 showed that neither MOFLUX_DroughtStress nor DroughtStress_ModelE altered the diurnal
 642 cycle in comparison to Default_ModelE. For 2011, all four simulations underestimate the diurnal
 643 cycle for MAY-AUG. Large improvements due to the applications of the Eq. (10a-10b) were not
 644 expected for 2011 as this algorithm was designed to target severe/extreme drought and not less
 645 severe drought conditions.

646
 647 During the severe drought period of 2012 at MOFLUX, the β values fell below the 4th
 648 percentile thresholds for July-August, and isoprene drought stress was applied leading to
 649 reductions in the overestimation shown by Default_ModelE. DroughtStress_ModelE had a MB
 650 $\cong 0.42$ mg/m²/hr and a NMB $\cong 14.5\%$ during the severe drought period. DroughtStress_ModelE
 651 reduced overestimation by $\sim 61.6\%$ during the severe drought period compared to
 652 Default_ModelE, which is a similar statistical improvement compared to
 653 MOFLUX_DroughtStress during the severe drought period as the parameterizations were
 654 designed in a similar manner. The scatterplots of isoprene emissions at the MOFLUX site for the
 655 summer of 2012 show the hourly correlation coefficient between observations and simulations
 656 increased from 0.68 in Default_ModelE to 0.73 in DroughtStress_ModelE (Fig. 2a,c). In Fig. 2
 657 changes are clearly seen in the cluster of β values lower than 0.4 (shown by red oval) indicating
 658 a reduction in overestimation during severe drought.
 659



660 Figure 2. Scatterplots (a-c) show hourly simulated isoprene emissions compared to observed for MAY-SEP 2012 at the
 661 MOFLUX site and the units are mg/m²/hr of isoprene. Column 1-3 indicate simulations Default_ModelE,
 662 DroughtStress_MEGAN3_Jiang, and DroughtStress_ModelE respectively. The hourly averaged points are color coded by
 663 water stress.

664
 665 DroughtStress_ModelE with decreases in y-intercept, increasing correlation coefficient, and
 666 minor change in slope compared to Default_ModelE suggests it has better performance in
 667 simulating isoprene emissions during severe and extreme drought at MOFLUX during the
 668 summer of 2012. The hourly scatterplots during the 2012 severe drought period are included in
 669 SI Fig. S13. The daily correlation coefficient increased from 0.64 to 0.73 during the 2012

670 drought in DroughtStress_ModelE (SI Fig. S5a,c) and in SI Fig. S13 during the severe drought
 671 period the daily correlation increases from 0.40 to 0.48. In addition, DroughtStress_ModelE
 672 reproduces the diurnal cycle of isoprene emission from MAY-SEP 2012 shown in (SI Fig. S4b)
 673 and corrects the overestimation of the Default_ModelE during the peak hours 10-15 LST. It was
 674 found that DroughtStress_ModelE tended to reduce the overestimation of Default_ModelE for
 675 the daily peak of isoprene flux and move it closer to observed during the severe drought period
 676 as shown in SI Fig. S9. Overall, there is an acceptable level of agreement between measured and
 677 modeled fluxes in DroughtStress_ModelE indicating it is a suitable model-tuned
 678 parameterization for estimating isoprene emissions during severe drought at the MOFLUX site.
 679

680 4. Model response to drought parameterization: Global/Regional Evaluation of 681 DroughtStress_ModelE

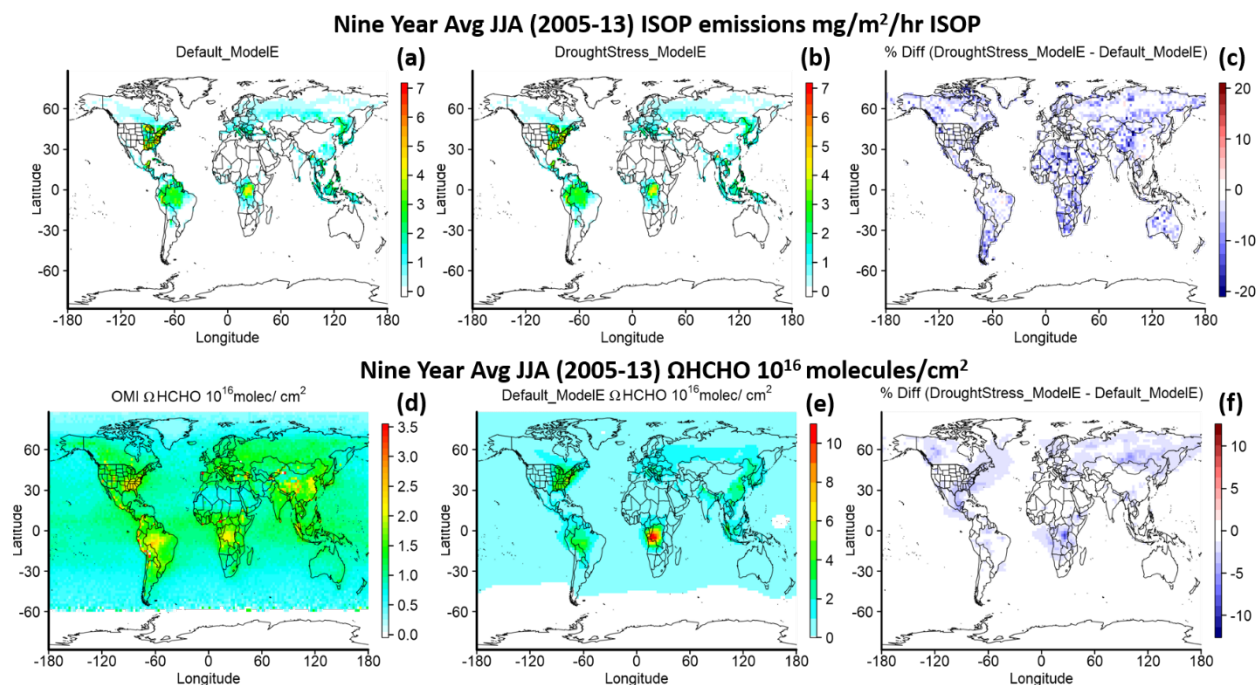
682 The impact of applying isoprene drought stress in DroughtStress_ModelE globally on the
 683 annual emissions of isoprene from 2003-2013 is shown in **Table 2**. The yearly global reduction
 684 of isoprene emissions ranges from $\sim -0.9\%$ to -4.3% . The global decadal average from 2003-
 685 2013 is $\sim 533 \text{ Tg yr}^{-1}$ of isoprene in Default_ModelE and $\sim 518 \text{ Tg yr}^{-1}$ of isoprene in
 686 DroughtStress_ModelE, a reduction of 2.7%, which is equivalent to $\sim 14.6 \text{ Tg yr}^{-1}$ of isoprene.
 687 On a global scale these changes average under 3%, but for high isoprene emission regions such
 688 as the Southeast U.S. during drought periods there are larger impacts as shown below in Fig. 6.
 689

690 **Table 2. Global Annual Tg of Isoprene (2003-2013)**

Global Annual Isoprene Emissions (Tg)				
Year	Default_ModelE	DroughtStress_ModelE	Diff (Tg Isoprene)	% Diff
2003	557.5	533.4	24.1	-4.3
2004	557.6	535.4	22.2	-4.0
2005	578.6	562.1	16.5	-2.9
2006	537.5	522.9	14.6	-2.7
2007	527.2	515.8	11.4	-2.2
2008	499.2	494.9	4.3	-0.9
2009	522.3	508.4	13.9	-2.7
2010	542.5	526	16.5	-3.0
2011	508.3	498.8	9.5	-1.9
2012	516.1	503.4	12.7	-2.5
2013	512.5	497.5	15	-2.9

691
 692 Figure 3 shows the global nine-year average of isoprene emissions and tropospheric HCHO
 693 column densities (ΩHCHO) of the lowest twenty layers of the model during JJA from 2005-
 694 2013. Due to extremely limited in situ measurements of isoprene emissions during drought,
 695 satellite-retrieved ΩHCHO , the high yield oxidation product of isoprene, can be used as a proxy
 696 for isoprene emissions on the monthly scale (Zhu *et al.* 2016). Here we used ΩHCHO from OMI

697 (Ozone Monitoring Instrument) on the Aura satellite starting in 2005. Level 3 total column
698 weighted mean was regridded from its original resolution of $0.1^\circ \times 0.1^\circ$ to match ModelE's
699 horizontal resolution of $2^\circ \times 2.5^\circ$, and the daily data was aggregated to monthly mean
700 (https://cmr.earthdata.nasa.gov/search/concepts/C1626121562-GES_DISC.html) (Chance 2019).
701 OMI satellite data was filtered with the data_quality_flag, cloud fractions less than 0.3, solar
702 zenith angles less than 60, and values within the range of -0.5 to 10×10^{16} molecules cm^{-2} were
703 used (Zhu *et al.* 2016). A factor of 1.59 is applied to the OMI vertical column density (VCD) to
704 correct the mean bias (Kaiser *et al.* 2018). As this is the first evaluation of tropospheric ΩHCHO
705 in ModelE, a gridded level 3 dataset was used for analysis without applying air mass factor
706 (AMF) using ModelE predicted HCHO profiles, which according to Zhu *et al.* (2016) can lead to
707 an increase in $\sim 38\%$ uncertainty in the southeast U.S.. Figures 3c,3f show the percent difference
708 of isoprene emissions and ΩHCHO and shown in blue are the decreases in
709 DroughtStress_ModelE globally. Figures 3d-e is OMI ΩHCHO and Default_ModelE simulated
710 ΩHCHO . It is important to note the difference in scales as Default_ModelE is overestimating
711 ΩHCHO in regions such as the SE U.S. for every June-July from the 2005-2013 period with a
712 regional mean scale factor of ~ 0.56 and ~ 0.80 when the SE boundary is extended westward to
713 include portions of Texas. These overestimates in the SE U.S. are also reported by (Kaiser *et al.*
714 2018) where they saw a 50% overestimate by GEOS-Chem with MEGAN2.1 simulations
715 compared to SEAC⁴RS observations. While applying isoprene drought stress leads to reductions
716 in ΩHCHO as shown by Fig. 3f, this reduction is limited to drought-stricken regions and periods
717 and not designed to correct for the systematic biases of HCHO in ModelE. The overestimation of
718 ΩHCHO in Default_ModelE will require further study and could be due to several reasons such
719 as emissions error, incorrect spatial gradient of OH, or possibly a too strong sensitivity to
720 temperature (Wells *et al.* 2020, Zhu *et al.* 2017, Wang *et al.* 2022).). This version of ModelE also
721 lacks direct emissions of HCHO from anthropogenic sources, which may result in the lower
722 vertical deposition, and, due to the short lifetime, the higher than observed HCHO column over
723 portions of the U.S., and lower in other regions. It was found that nudged simulations show a
724 large overestimation of HCHO column compared to free-running simulations using model winds.
725 As this study only shows modest decreases in HCHO column we can only conclude that adding
726 isoprene drought stress into a model may reduce HCHO column depending on atmospheric
727 chemistry, but under certain NO_x and VOC limited environments may have another effect.

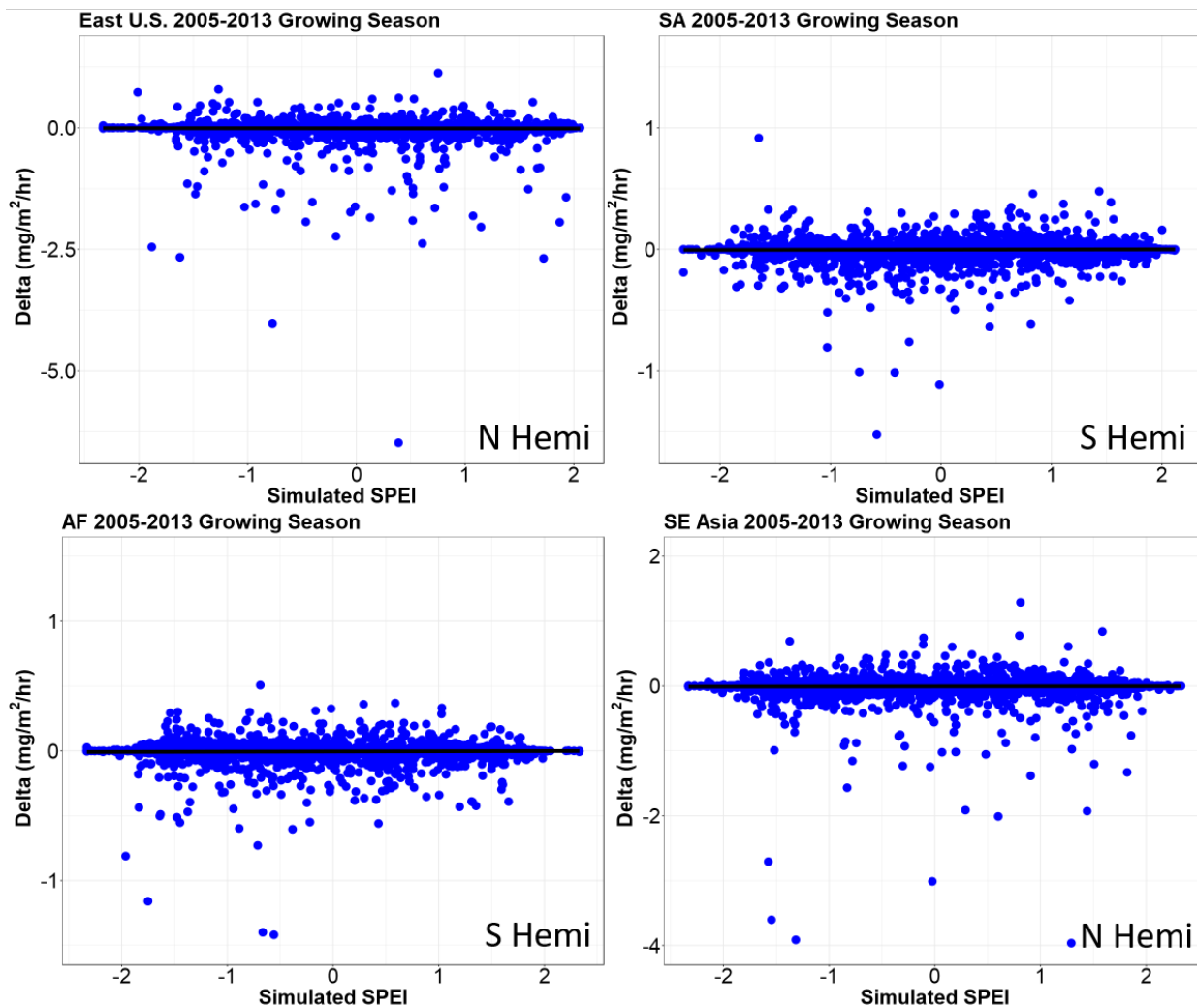


729 **Figure 3. Global nine-year average of JJA from 2005-2013 of isoprene emissions (first row) for Default_ModelE (a),**
 730 **DroughtStress_ModelE (b) and percent difference between DroughtStress_ModelE and Default_ModelE (c), and**
 731 **ΩHCHO (second row) for OMI (d), Default_ModelE (e) and percent difference between DroughtStress_ModelE and**
 732 **Default_ModelE (f). Note the different color scales between (d) and (e).**

733
 734 Four global isoprene emission hotspots are selected to showcase the changes in isoprene
 735 emissions. The geographic regions are defined as East U.S. (Eastern U.S.: 65-105°W, 25-50°N),
 736 SA (Amazon: 40-80°W, 30°S-7°N), AF (Central Africa: 10-40°E, 15°S-10°N), and SE Asia
 737 (Southeast Asia: 100-150°E, 11°S-38°N) as shown in (SI Fig. S6). Figure 4 shows the
 738 relationship of dryness categorized by SPEI (Standardized Precipitation-Evapotranspiration
 739 Index) and relative difference in isoprene emissions between DroughtStress_ModelE and
 740 Default_ModelE from 2005-2013 for the growing season in the northern hemisphere and
 741 spring/summer in the southern hemisphere for the four global isoprene hotspots. SPEI is a
 742 multiscalar climatic index that represents duration of drought in a region and is based on a
 743 climatic water balance approach which considers the impact of temperature and
 744 evapotranspiration (Beguería *et al.* 2010; Vicente-Serrano *et al.* 2010; Beguería *et al.* 2014). To
 745 identify the extent of drought impacts and differentiate from normal variability in the
 746 hydrological cycle, one-month SPEI is used to identify drought periods of duration extending
 747 beyond a single month. Default_ModelE simulation variables were used to calculate modeled
 748 SPEI at the resolution of 2°×2.5°. Positive SPEI typically indicates wet conditions and dry
 749 conditions are indicated by negative values. Drought conditions are indicated by SPEI ≤ -1.3,
 750 normal conditions -0.5 ≤ SPEI ≤ 0.5, and wet conditions SPEI ≥ 1.3 following the (Wang *et al.*
 751 2017) approach. For the four regions the average percent difference in isoprene emissions for

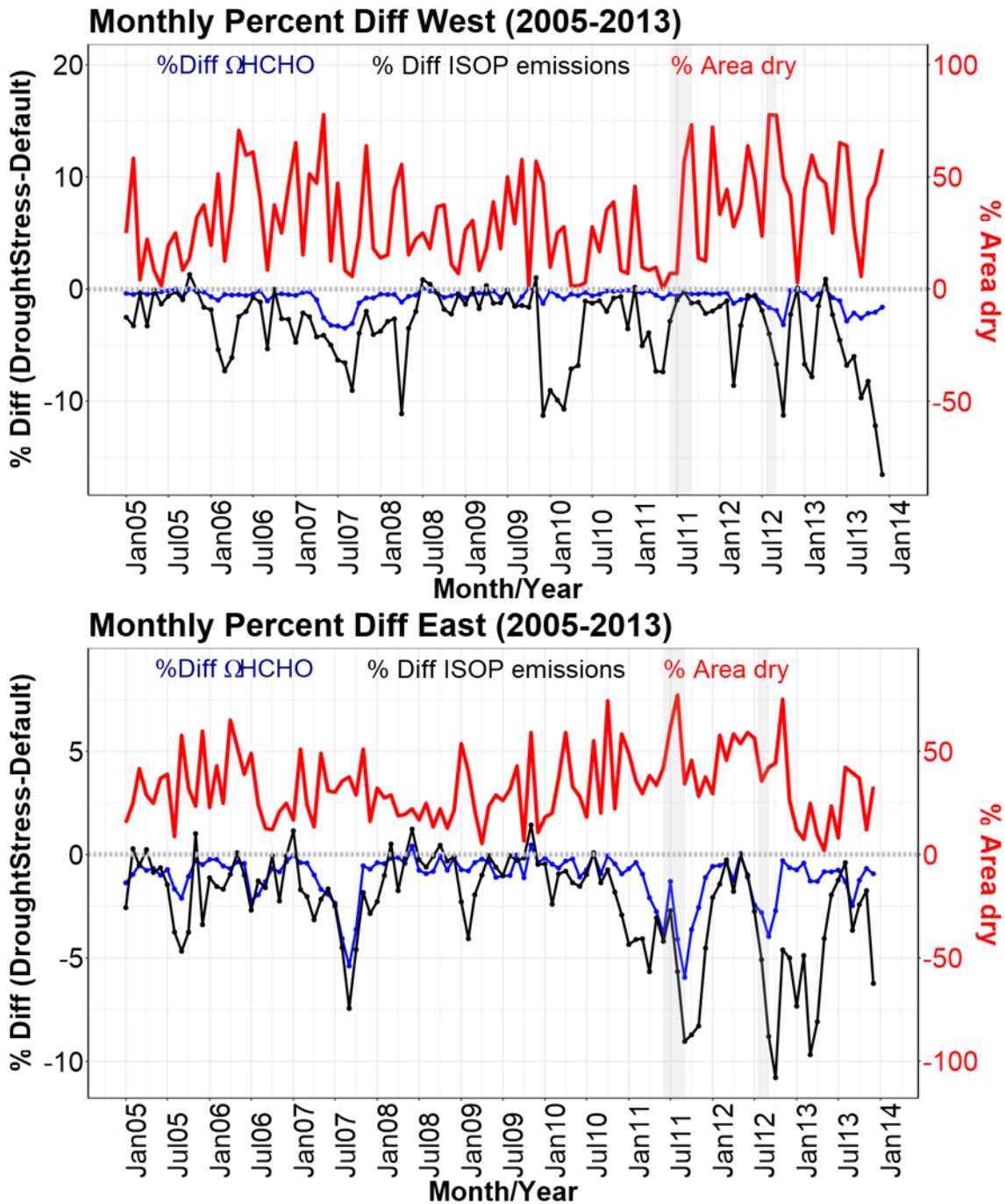
752 March-October for northern hemisphere regions and September-February for southern
 753 hemisphere regions from 2005-2013 is $\sim -2.62\%$ for the East U.S., the Amazon (SA) $\sim -3.01\%$,
 754 Central Africa (AF) $\sim -2.64\%$, and Southeast Asia (SE Asia) $\sim -3.10\%$. The scatterplots for the
 755 four hotspots show decreasing isoprene emissions across all dryness conditions. The decreases in
 756 isoprene emissions for the four regions are not seen exclusively when SPEI indicates dry
 757 conditions, which indicates simulated water stress as shown by model does not align exactly with
 758 SPEI drought indicated conditions.
 759

2005 - 2013 SPEI vs ISOP Delta (DroughtStress_ModelE-Default_ModelE)



760 **Figure 4.** The scatterplots of four global isoprene hotspot and their relative differences in isoprene emissions (mg/m²/hr
 761 isoprene) in relationship to simulated SPEI from 2005-2013 during the growing season is shown. The four regions of focus
 762 are Eastern U.S. (East), Amazon (SA), Central Africa (AF), and Southeast Asia (SE Asia). The regions of East and SE
 763 Asia are in the northern hemisphere and the growing seasons is from (March-October). The hotspots of SA and AF are in
 764 the southern hemisphere and the growing season is during spring/summer (September-February).
 765

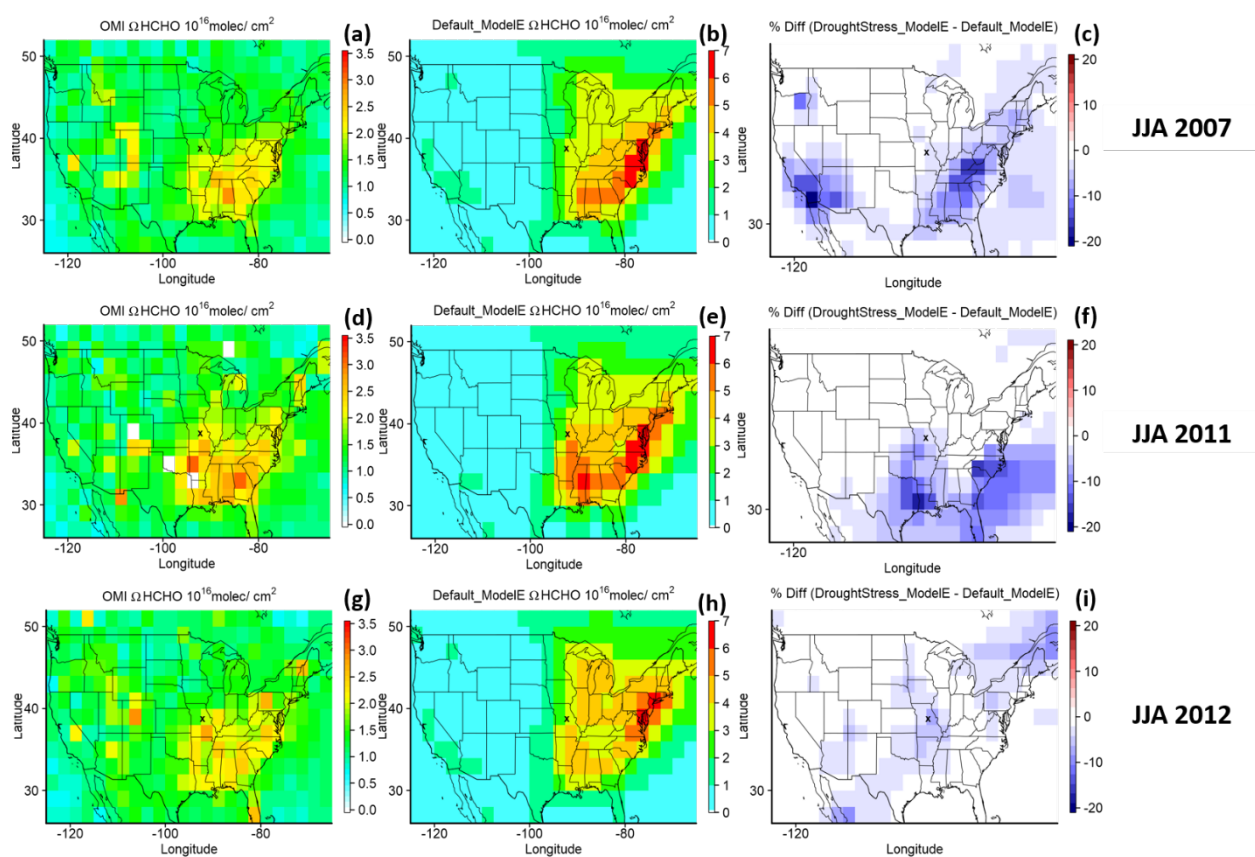
766 Narrowing the focus from global to the U.S., to illustrate the long-term difference between
767 DroughtStress_ModelE and Default_ModelE, a timeseries from 2005-2013 is shown in Fig. 5 of
768 the continental U.S. for two regions West (105-125°W, 25-50°N) and East (65-105°W, 25-50°N)
769 indicating the percent difference in Ω HCHO and isoprene emissions corresponding to percent
770 area that is dry (SPEI < -0.5). The map showing the regions West and East is located in (SI Fig.
771 S7). The western U.S. (West) despite having a much smaller magnitude of isoprene emissions
772 does see reductions in isoprene which is mimicked on a lesser scale by reductions in Ω HCHO.
773 For the Eastern U.S. (East) there are visible decreases in the percent reduction of isoprene
774 emission and Ω HCHO during the 2007, 2011, and 2012 drought years. Focusing on the East
775 timeseries, the maximum percent difference between simulations DroughtStress_ModelE and
776 Default_ModelE for isoprene occurred from AUG-OCT 2007 approximately -4.5%, -7.4%, and -
777 4.6% with corresponding decreases in Ω HCHO of ~ -4.1%, -5.4%, and -3.6% respectively. For
778 2011 the maximum percent difference in isoprene emissions occurred SEP-NOV and was ~ -
779 9.0%, -8.7%, -8.3% and the percent difference in Ω HCHO was ~ -5.9%, -3.6%, and -2.6%. For
780 2012 the maximum percent difference occurred from AUG-OCT and the difference in isoprene
781 was ~ -5.1%, -8.8%, and -10.8% and the difference in Ω HCHO was ~ -2.8%, -4.0%, and -2.7%.
782



783 Figure 5. The percent difference of Ω HCHO and isoprene emissions from 2005-2013 in relationship to percent area dry
 784 for two regions of the U.S. West (top figure) and East (bottom figure) is shown. Percent area dry is indicated by SPEI < -
 785 0.5. The first grey shaded rectangle indicates the time period of the 2011 drought at MOFLUX from June to August 2011.
 786 The second grey shaded rectangle indicates the 2012 severe drought at MOFLUX from July 17 through August. These
 787 time periods are added to the timeseries to highlight when they occurred.
 788

789 Figure 6 displays spatial maps of Ω HCHO during the summer (JJA) of three drought years
 790 2007, 2011, and 2012. The summers of 2007 and 2011 were drought periods in the U.S. with

791 2007 being a less severe drought than 2011 in the SE U.S. The drought of 2012 was focused
 792 more on the Great Plains (GP) region. The spatial maps show the reduction in ΩHCHO in panels
 793 6c, 6f, and 6i due to the inclusion of isoprene drought stress. Based on the spatial differences in
 794 ΩHCHO , three regions of the greatest reduction in percent difference in ΩHCHO column are
 795 selected for the three drought years of 2007, 2011, and 2012, respectively. The three geographic
 796 regions are shown in Fig. 7 and defined as SE1(Southeast Region1: 75-93°W, 31-39°N), SE2
 797 (Southeast Region2: 75-101°W, 29-37°N), and GP (Great Plains: 89-100°W, 33-43°N). During
 798 JJA for 2007 the SE1 region has an average percent difference in ΩHCHO of -6.46%, during JJA
 799 2011 the SE2 region has a percent difference of -7.58%, and the GP region during JJA 2012 has
 800 average percent difference of -3.29%.
 801



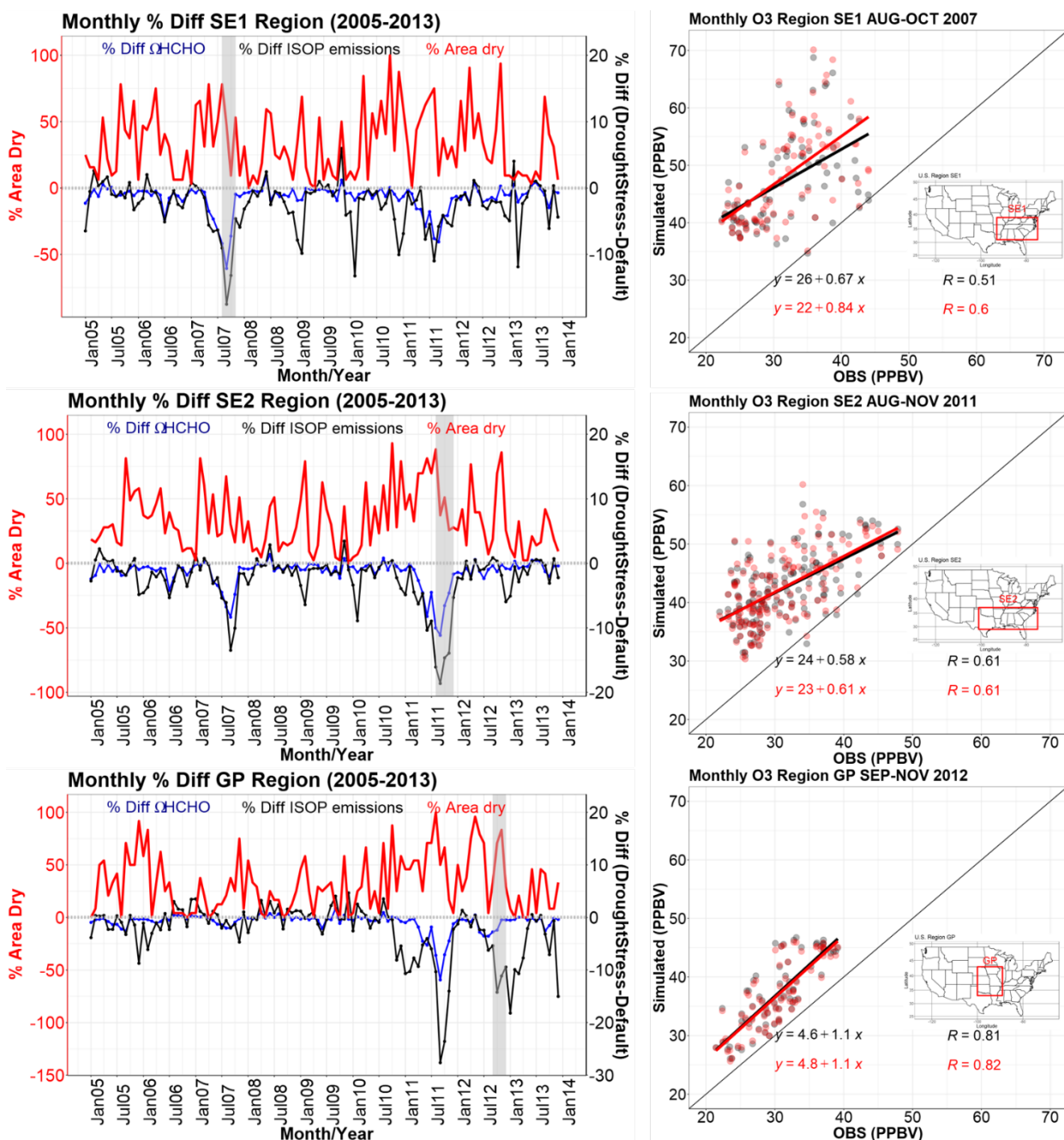
802 **Figure 6. The ΩHCHO column in units of molecules/cm² for OMI, Default_ModelE, and the percent difference between**
 803 **DroughtStress_ModelE and Default_ModelE across the U.S. during the summer of drought years 2007, 2011, and 2012 is**
 804 **shown. X indicates the location of the MOFLUX site on the spatial maps.**
 805

806 Figure 7 shows the timeseries for the three regions of SE1 during 2007, SE2 for 2011, and
 807 GP for 2012 drought. In the SE1 region during the period of maximum isoprene difference from
 808 AUG-OCT 2007 shaded in grey on the timeseries, DroughtStress_ModelE reduced NMB of
 809 ΩHCHO by ~19.3%. The isoprene percent difference for this period was approximately -9.0%, -
 810 17.5%, and -13.2%. The ΩHCHO percent difference for the SE1 region from AUG-OCT 2007

811 was approximately -8.4%, -12.1%, and -7.3%. In the SE2 region the maximum isoprene
812 difference period for AUG-NOV 2011, DroughtStress_ModelE decreased Ω HCHO NMB by
813 \sim 15.3%. The monthly isoprene percent difference for SE2 during this period was approximately
814 -16.1%, -18.6%, -14.7%, and -13.9% while the Ω HCHO percent difference was \sim -10.0%, -
815 11.2%, -6.6%, and -4.6% respectively. In the GP region during SEP-NOV 2012, the isoprene
816 percent difference for GP during SEP-NOV 2012 was approximately -5.4%, -14.2%, and -11.1%
817 and the Ω HCHO percent difference was \sim -2.8%, -2.4%, and -0.4% respectively. The small
818 change in HCHO column despite estimated larger changes in isoprene emissions is probably due
819 to the suppression of oxidants such as hydroxyl radicals (OH) by isoprene under low-NO_x
820 conditions in the GP region (Wells *et al.* 2020).

821
822 It is well established that biogenic isoprene, the most abundant BVOC, is a highly reactive
823 species. In the presence of nitrogen oxides (NO_x), BVOCs contribute to the formation of
824 tropospheric O₃. Oxidation of BVOCs also produces secondary organic aerosols, a major
825 component of fine particulate matter (PM_{2.5}). PM_{2.5} and O₃ have been previously linked to
826 change during drought with adverse effects on air quality (Wang *et al.* 2017). During drought
827 there is elevated O₃ and PM_{2.5}, compared to non-drought periods (Wang *et al.* 2017; Zhao *et al.*
828 2019; Naimark *et al.*, 2021). Higher ozone compared to non-drought years is due to the reduction
829 of vegetative deposition due to reduced stomatal conductance, higher temperatures stimulating
830 precursors, and enhanced NO₂ (Naimark *et al.* 2021). By including isoprene drought stress into
831 the simulations, isoprene emissions are decreased which will change O₃, the direction of change
832 depends on NO_x-limited or VOC-limited regimes (Li *et al.* 2022). In summary, we better
833 predicted isoprene emission response to drought by including isoprene drought stress. It is thus
834 important to show the impact of drought-induced changes in isoprene emissions on O₃ and
835 PM_{2.5}. The scatterplots in Fig. 7 show the relationship between observed and simulated O₃ during
836 the drought period of maximum percent difference highlighted on the timeseries for the
837 corresponding region. PM_{2.5} comparison to observed is not shown here due to Default_ModelE
838 underestimating PM_{2.5} across all three regions SE1, SE2, and GP, and thus no improvements
839 were seen due to the inclusions of DroughtStress_ModelE. The observational O₃ data is a
840 combination of hourly data from the EPA-AQS (U.S. Environmental Protection Agency (EPA)
841 Air Quality System), CASTNET (Clean Air Status and Trends Network), and NAPS (National
842 Air Pollution Surveillance) networks. The observational O₃ datasets was gridded and interpolated
843 for comparison to a gridded model (Schnell *et al.* 2014). The hourly gridded observations were
844 then averaged onto a monthly scale for comparison with model results. Shown in Fig. 7 the SE1
845 region saw improvement in O₃ from AUG-OCT 2007, where the correlation coefficient (R)
846 increased from 0.51 in Default_ModelE to 0.60 in DroughtStress_ModelE and the slope of the
847 linear regression also improved significantly. The SE2 region from AUG-NOV 2011 saw a slight
848 improvement in the slope of the linear regression but no change in R. The GP region from SEP-
849 NOV 2012 saw a slight improvement in R but no change in the correlation slope between
850 Default_ModelE and DroughtStress_ModelE. During non-drought periods of 2008, 2010, and

851 2013 compared to their respective drought periods of 2007, 2011, and 2012 there was no large
 852 changes in O₃ or ΩHCHO statistics as expected since isoprene drought stress is only supposed to
 853 affect drought periods. During the drought periods of 2007, 2011, and 2012 the model predicts
 854 higher mean O₃ and ΩHCHO than the non-drought years of 2008, 2010, and 2013. The analysis
 855 of these drought years and periods of the greatest percent difference leads to the conclusion of
 856 isoprene drought stress improves ΩHCHO simulation and O₃ simulation during drought periods.
 857



858 **Figure 7. The timeseries from 2005-2013 of percent area dry on y-axis shown in red and percent difference in ΩHCHO**
 859 **(blue) and isoprene emissions (black) between DroughtStress_ModelE and Default_ModelE for the 3 regions SE1, SE2,**

860 and GP on the second y-axis is shown. Shaded in grey are the time periods of maximum percent difference of isoprene
861 emissions during the drought years. The scatterplots show the relationship between observed O₃ (ppbv) and simulated O₃
862 during the shaded grey time periods on the timeseries for Default_ModelE in black and DroughtStress_ModelE in red for
863 the SE1 during 2007, SE2 during 2011, and GP during 2012. Maps showing the geographic regions are inset into the
864 scatterplots. The regions spatial extent is based on region of maximum percent difference in Fig. 6c,f,i.

865

866 5. Discussion and conclusions

867 Drought is a hydroclimatic extreme that causes perturbations to the terrestrial biosphere. As a
868 stressor for vegetation, drought can induce changes to vegetative emissions known as BVOCs
869 (Biogenic Volatile Organic Compounds). Biogenic isoprene represents about half of total BVOC
870 emissions and is a precursor to ozone (O₃) and secondary organic aerosol (SOA), both of which
871 are climate forcing species. In order to simulate isoprene flux during drought and the feedbacks
872 associated with these complex BVOC-chemistry-climate interactions, we implemented the
873 MEGAN (Model of Emissions of Gases and Aerosols from Nature) isoprene drought stress
874 parameterization, y_d , into NASA GISS (Goddard Institute of Space Studies) ModelE, a leading
875 Earth System Model. Four online transient simulations were performed from 2003-2013, a
876 Default_ModelE without y_d , DroughtStress_MEGAN3_Jiang using the parameterization
877 developed by (Jiang *et al.* 2018), and a model-tuned parameterization developed for ModelE
878 based on the MOFLUX Ameriflux site observations (MOFLUX_DroughtStress). The fourth
879 simulation implemented isoprene drought stress using a grid-by-grid approach to capture
880 regional changes in isoprene during drought known as DroughtStress_ModelE. The model-tuned
881 parameterization (MOFLUX_DroughtStress and DroughtStress_ModelE) was developed using
882 an offline model of emissions to create a model specific empirical variable and water stress
883 threshold, since key variables $V_{c,max}$ (photosynthetic parameter) and water stress (β) are
884 parameterized differently across models. Observational measurements of isoprene flux during
885 the severe drought of 2012 at the MOFLUX site were used for validation of parameterization. It
886 was found that DroughtStress_ModelE corrects the overestimation of emissions during the phase
887 of severe drought at MOFLUX. Previously, this reduction during drought was not included in
888 BVOC emission models due to the lack of a drought stress term. Globally the decadal average
889 from 2003-2013 in Default_ModelE was ~533 Tg of isoprene and ~518 Tg of isoprene in
890 DroughtStress_ModelE. DroughtStress_ModelE was validated using observational satellite
891 Ω HCHO column from the Ozone Monitoring Instrument (OMI) and using O₃ observations
892 across regions of the U.S. to examine the effect of drought on atmospheric composition. It was
893 found that the inclusion of isoprene drought stress reduced the overestimation of Ω HCHO in
894 Default_ModelE during the 2007 and 2011 southeastern U.S. droughts and led to improvements
895 in simulated O₃ during drought periods. The inclusions of a grid specific percentile isoprene
896 drought stress is model specific and the reduction of isoprene seen in models will depend on each
897 models mean bias and parameterizations of $V_{c,max}$ and water stress. ModelE's modest signal can
898 be explained by underestimating isoprene emissions during the early stages of drought and by
899 not having a high mean bias during severe drought.

900
901 Our analysis of isoprene drought stress leads to the recommendation that each model should
902 arrive at a tuning of their water stress parameters based on the magnitude of water stress
903 occurring during simulated drought and a unique alpha should be derived. Each land surface
904 model (LSM) has a unique hydrology scheme (with different soil layering approaches and soil
905 physics treatments), and any variables that depend on response to soil moisture -- whether
906 chemical, physical, or biological -- must be tuned due to the fact that soil moisture in LSMs is
907 being averaged over a grid cell whereas in nature soil moisture is heterogeneous at spatial scales
908 down to the plot level. The resulting parameterization, since it relies on model specific variables,
909 would be well suited for future or historical simulations. The current approach also requires
910 vegetation-coupled land surface models that have photosynthesis models that use $V_{c,max}$ and β ,
911 and many current general circulation models (GCM) with less process-based vegetation schemes
912 do not have these variables readily available.

913
914 Besides tuning responses to drought, the light response of isoprene emissions may not be
915 well captured in a simple factor like the PCEEA. Vegetation models differ in their approach to
916 leaf-to-canopy scaling. Some ESMs vegetation models have more sophisticated canopy radiative
917 transfer submodels that capture layering and sunlit/shaded leaf area. Future isoprene modeling
918 investigations could make use of the ability of these canopy models to calculate isoprene
919 emissions with leaf-level responses to the heterogeneous light in canopies. Unger *et al.* (2013)
920 implemented such a leaf-to-canopy scaling of isoprene emissions previously in the Ent TBM
921 through a leaf-level isoprene model as a function of leaf-level gross primary production (GPP).
922 Since the Ent TBM scales stomatal conductance with drought stress, and hence also GPP, this
923 intrinsically results in isoprene emissions responsiveness to drought stress. The main challenge
924 will be to find consensus about the fundamental process-based physics of isoprene emissions
925 at the leaf level. The method of Unger *et al.* (2013) was not used for this paper in order to
926 preserve the MEGAN3 features and test this particular isoprene drought stress parameterization.

927
928 A limitation of our tuning method for applying isoprene drought stress is that there does not
929 appear to be a strong relationship between SPEI and water stress, which makes it challenging to
930 determine when the algorithm should be applied during severe drought. This is why the current
931 application is limited and based on the single MOFLUX site where water stress values and the
932 corresponding decreases of isoprene during severe drought were observed. Possible future work
933 of the satellite Cross-track Infrared Sound (CrIS) isoprene measurements (Wells *et al.* 2020)
934 may be used to develop a drought algorithm that is not based on a single site and provide a more
935 dynamic drought stress algorithm for capturing the decrease of emissions during severe drought.
936 The reduction of isoprene in the model also depends on how dry (low values of water stress) the
937 model is. If the model is too dry or if isoprene emissions are already overestimated there will be
938 larger reductions in isoprene than reported here in ModelE, with larger feedbacks on O₃, SOA,
939 and ΩHCHO column. Models that are not severely overestimating during severe drought will

940 show modest reductions like ModelE. It is important to note that the application of isoprene
941 drought stress in this paper is designed to reduce emissions during severe drought. Future work
942 could focus more on the parameterization of isoprene emissions during mild or early stages of
943 drought when isoprene emissions might be increasing and as we see in ModelE the model
944 underestimates during this period. Overall, the strength of the reduction signal of isoprene
945 depends on the model, and for models overestimating isoprene the application of isoprene
946 drought stress into the model could improve model simulations significantly. Recent published
947 work has also brought up the importance of drought duration as an important factor to consider
948 in further isoprene drought stress parameterization (Li *et al.* 2022). Future work on developing
949 drought parameterizations should focus on capturing the increasing signal of isoprene at the start
950 of drought, the reduction signal during severe drought, while also considering a time component
951 because eventually plants can reach a stage of emission cessation.

952
953 In summary, this paper demonstrates why isoprene response to drought stress is model
954 specific and should be tuned on a model-by-model basis, and details a new method for
955 implementing isoprene drought stress to reduce isoprene emissions during severe drought in
956 ModelE. This new method uses a grid-by-grid percentile threshold based on simulated water
957 stress and can be used by many models to show regional changes in isoprene emissions during
958 severe drought and their associated feedbacks on ΩHCHO and O_3 . With more severe droughts
959 predicted in the United States for the 21st century (Dai 2013), this is a first look into model
960 performance for analyzing how BVOC emissions change during drought conditions using GISS
961 ModelE for regions in the U.S.

962 **6. Acknowledgements**

963 E.K., Y.W. and A.G. would like to acknowledge the support and funding from the NASA
964 ACPMAP Program (80NSSC19K0986). E.K. and Y.W. would also like to acknowledge the
965 support and funding of NASA Fellowship Grant (80NSSC18K1704) and thank support of NASA
966 technical advisors at Goddard Institute of Space Studies. Resources supporting this work were
967 provided by the NASA High-End Computing (HEC) Program through the NASA Center for
968 Climate Simulation (NCCS) at the Goddard Space Flight Center. GISS authors acknowledge
969 funding from the NASA Modeling and Analysis program.

970 **7. Data availability**

971 ModelE is publicly available at <https://simplex.giss.nasa.gov/snapshots/> and O_3 and $\text{PM}_{2.5}$
972 observational data available for download via
973 https://aqs.epa.gov/aqswweb/documents/data_mart_welcome.html. Observational isoprene
974 measurements at MOFLUX are from Potosnak *et al.* 2014 and Seco *et al.* 2015 and are available
975 upon request from co-author Alex Guenther. MOFLUX is part of the Ameriflux network and
976 other observational data is available for download at [https://ameriflux.lbl.gov/sites/siteinfo/US-](https://ameriflux.lbl.gov/sites/siteinfo/US-MOz#BADM)
977 [MOz#BADM](https://ameriflux.lbl.gov/sites/siteinfo/US-MOz#BADM). Satellite ΩHCHO is available publicly at
978 https://cmr.earthdata.nasa.gov/search/concepts/C1626121562-GES_DISC.html.

981 **8. Author contribution**

983 EK and YW conceived the research idea. EK wrote the initial draft, conducted the simulations,
984 and performed the analysis. EK and GF conducted model development. All authors contributed
985 to the interpretation of the results and the preparation of the paper.

986

987 **9. Competing interests**

988 The authors declare that they have no conflict of interest.

989

990 **References**

- 991 Arneth, A., Monson, R. K., Schurgers, G., Niinemets, Ü. and Palmer, P. I.: Why are estimates of
992 global terrestrial isoprene emissions so similar (and why is this not so for monoterpenes)?,
993 Atmospheric Chemistry and Physics, 8(16), 4605–4620, doi:10.5194/acp-8-4605-2008, 2008.
994
- 995 Ball, T. and Berry, J.: A Simple Empirical Model of Stomatal Control. Plant Physiology 77(n.
996 Supplement 4): 91, 1985.
- 997
- 998 Bauer, S. E., Mishchenko, M. I., Lacis, A. A., Zhang, S., Perlwitz, J. and Metzger, S. M.: Do
999 sulfate and nitrate coatings on mineral dust have important effects on radiative properties and
1000 climate modeling?, Journal of Geophysical Research, 112(D6), doi:10.1029/2005jd006977,
1001 2007.
1002
- 1003 Bauer, S. E., Tsigaridis, K., Faluvegi, G., Kelley, M., Lo, K. K., Miller, R. L., Nazarenko, L.,
1004 Schmidt, G. A. and Wu, J.: Historical (1850–2014) Aerosol Evolution and Role on Climate
1005 Forcing Using the GISS ModelE2.1 Contribution to CMIP6, Journal of Advances in Modeling
1006 Earth Systems, 12(8), doi:10.1029/2019ms001978, 2020.
1007
- 1008 Bauer, S. E., Wright, D. L., Koch, D., Lewis, E. R., Mcgraw, R., Chang, L.-S., Schwartz, S. E.
1009 and Ruedy, R.: MATRIX (Multiconfiguration Aerosol TRacker of mIXing state): an aerosol
1010 microphysical module for global atmospheric models, Atmospheric Chemistry and Physics,
1011 8(20), 6003–6035, doi:10.5194/acp-8-6003-2008, 2008.
1012
- 1013 Beguería, S., Vicente-Serrano, S. M. and Angulo-Martínez, M.: A Multiscalar Global Drought
1014 Dataset: The SPEIbase: A New Gridded Product for the Analysis of Drought Variability and
1015 Impacts, Bulletin of the American Meteorological Society, 91(10), 1351–1356,
1016 doi:10.1175/2010bams2988.1, 2010.
1017
- 1018 Beguería, S., Vicente-Serrano, S. M., Reig, F. and Latorre, B.: Standardized precipitation
1019 evapotranspiration index (SPEI) revisited: parameter fitting, evapotranspiration models, tools,
1020 datasets and drought monitoring, International Journal of Climatology, 34(10), 3001–3023,
1021 doi:10.1002/joc.3887, 2014.
1022
- 1023 Benjamin, M. T., Sudol, M., Bloch, L. and Winer, A. M.: Low-emitting urban forests: A
1024 taxonomic methodology for assigning isoprene and monoterpene emission rates, Atmospheric
1025 Environment, 30(9), 1437–1452, doi:10.1016/1352-2310(95)00439-4, 1996.
1026

1027 Carlton, A. G., Wiedinmyer, C. and Kroll, J. H.: A review of Secondary Organic Aerosol (SOA)
1028 formation from isoprene, *Atmospheric Chemistry and Physics*, 9(14), 4987–5005,
1029 doi:10.5194/acp-9-4987-2009, 2009.

1030
1031 Chance, K.: OMI/Aura Formaldehyde (HCHO) Total Column Daily L3 Weighted Mean Global
1032 0.1deg Lat/Lon Grid V003, Greenbelt, MD, USA, Goddard Earth Sciences Data and Information
1033 Services Center (GES DISC), Accessed: [2021-04-07], 10.5067/Aura/OMI/DATA3010, 2019.

1034
1035 Clapp, R. B. and Hornberger, G. M.: Empirical equations for some soil hydraulic properties,
1036 *Water Resources Research*, 14(4), 601–604, doi:10.1029/wr014i004p00601, 1978.

1037
1038 Dai, A.: Increasing drought under global warming in observations and models, *Nature Climate*
1039 *Change*, 3(1), 52–58, doi:10.1038/nclimate1633, 2013.

1040
1041 Emmerson, K. M., Palmer, P. I., Thatcher, M., Haverd, V. and Guenther, A. B.: Sensitivity of
1042 isoprene emissions to drought over south-eastern Australia: Integrating models and satellite
1043 observations of soil moisture, *Atmospheric Environment*, 209, 112–124,
1044 doi:10.1016/j.atmosenv.2019.04.038, 2019.

1045
1046 Farquhar, G. D. and von Caemmerer, S.: Modelling of Photosynthetic Response to
1047 Environmental Conditions. *Physiological Plant Ecology II: Water Relations and Carbon*
1048 *Assimilation*. O. L. Lange, P. S. Nobel, C. B. Osmond and H. Ziegler. Berlin, Heidelberg,
1049 Springer Berlin Heidelberg: 549-587, 1982.

1050 Geron, C., Guenther, A., Sharkey, T. and Arnts, R. R.: Temporal variability in basal isoprene
1051 emission factor, *Tree Physiology*, 20(12), 799–805, doi:10.1093/treephys/20.12.799, 2000.

1052
1053 Gu, L., Meyers, T., Pallardy, S.G., Hanson, P.J., Yang, B., Heuer, M., Hosman, K.P., Riggs, J.S.,
1054 Sluss, D., Wullschlegel, S.D., 2006. Direct and indirect effects of atmospheric conditions and
1055 soil moisture on surface energy partitioning revealed by a prolonged drought at a temperate
1056 forest site. *Journal of Geophysical Research: Atmospheres* 111.. doi:10.1029/2006jd007161.

1057
1058 Guenther, A., Karl, T., Harley, P., Wiedinmyer, C., Palmer, P. I. and Geron, C.: Estimates of
1059 global terrestrial isoprene emissions using MEGAN (Model of Emissions of Gases and Aerosols
1060 from Nature), *Atmospheric Chemistry and Physics*, 6(11), 3181–3210, doi:10.5194/acp-6-3181-
1061 2006, 2006.

1062
1063 Guenther, A. B., Jiang, X., Heald, C. L., Sakulyanontvittaya, T., Duhl, T., Emmons, L. K. and
1064 Wang, X.: The Model of Emissions of Gases and Aerosols from Nature version 2.1
1065 (MEGAN2.1): an extended and updated framework for modeling biogenic emissions,
1066 *Geoscientific Model Development*, 5(6), 1471–1492, doi:10.5194/gmd-5-1471-2012, 2012.

1067
1068 Heald, C. L., Wilkinson, M. J., Monson, R. K., Alo, C. A., Wang, G. and Guenther, A.:
1069 Response of isoprene emission to ambient CO₂ changes and implications for global budgets,
1070 *Global Change Biology*, 15(5), 1127–1140, doi:10.1111/j.1365-2486.2008.01802.x, 2009.

1071

1072 Henrot, A.-J., Stanelle, T., Schröder, S., Siegenthaler, C., Taraborrelli, D. and Schultz, M. G.:
1073 Implementation of the MEGAN (v2.1) biogenic emission model in the ECHAM6-HAMMOZ
1074 chemistry climate model, *Geoscientific Model Development*, 10(2), 903–926, doi:10.5194/gmd-
1075 10-903-2017, 2017.

1076
1077 Hoesly, R. M., Smith, S. J., Feng, L., Klimont, Z., Janssens-Maenhout, G., Pitkanen, T., Seibert,
1078 J. J., Vu, L., Andres, R. J., Bolt, R. M., Bond, T. C., Dawidowski, L., Kholod, N., Kurokawa, J.-
1079 I., Li, M., Liu, L., Lu, Z., Moura, M. C. P., O'Rourke, P. R. and Zhang, Q.: Historical (1750–
1080 2014) anthropogenic emissions of reactive gases and aerosols from the Community Emissions
1081 Data System (CEDS), *Geoscientific Model Development*, 11(1), 369–408, doi:10.5194/gmd-11-
1082 369-2018, 2018.

1083
1084 Huang, L., Mcgaughey, G., McDonald-Buller, E., Kimura, Y. and Allen, D. T.: Quantifying
1085 regional, seasonal and interannual contributions of environmental factors on isoprene and
1086 monoterpene emissions estimates over eastern Texas, *Atmospheric Environment*, 106, 120–128,
1087 doi:10.1016/j.atmosenv.2015.01.072, 2015.

1088
1089 Ito, G., Romanou, A., Kiang, N. Y., Faluvegi, G., Aleinov, I., Ruedy, R., Russell, G., Lerner, P.,
1090 Kelley, M. and Lo, K.: Global Carbon Cycle and Climate Feedbacks in the NASA GISS
1091 ModelE2.1, *Journal of Advances in Modeling Earth Systems*, 12(10),
1092 doi:10.1029/2019ms002030, 2020.

1093
1094 Jiang, X., Guenther, A., Potosnak, M., Geron, C., Seco, R., Karl, T., Kim, S., Gu, L. and
1095 Pallardy, S.: Isoprene emission response to drought and the impact on global atmospheric
1096 chemistry, *Atmospheric Environment*, 183, 69–83, doi:10.1016/j.atmosenv.2018.01.026, 2018.

1097
1098 Kaiser, J., Jacob, D. J., Zhu, L., Travis, K. R., Fisher, J. A., González Abad, G., Zhang, L.,
1099 Zhang, X., Fried, A., Crouse, J. D., St. Clair, J. M. and Wisthaler, A.: High-resolution inversion
1100 of OMI formaldehyde columns to quantify isoprene emission on ecosystem-relevant scales:
1101 application to the southeast US, *Atmospheric Chemistry and Physics*, 18(8), 5483–5497,
1102 doi:10.5194/acp-18-5483-2018, 2018.

1103
1104 Kelley, M., Schmidt, G. A., Nazarenko, L. S., Bauer, S. E., Ruedy, R., Russell, G. L., Ackerman,
1105 A. S., Aleinov, I., Bauer, M., Bleck, R., Canuto, V., Cesana, G., Cheng, Y., Clune, T. L., Cook,
1106 B. I., Cruz, C. A., Del Genio, A. D., Elsaesser, G. S., Faluvegi, G., Kiang, N. Y., Kim, D., Lacis,
1107 A. A., Leboissetier, A., Legrande, A. N., Lo, K. K., Marshall, J., Matthews, E. E., Mcdermid, S.,
1108 Mezuman, K., Miller, R. L., Murray, L. T., Oinas, V., Orbe, C., García-Pando, C. P., Perlwitz, J.
1109 P., Puma, M. J., Rind, D., Romanou, A., Shindell, D. T., Sun, S., Tausnev, N., Tsigaridis, K.,
1110 Tselioudis, G., Weng, E., Wu, J. and Yao, M.: GISS-E2.1: Configurations and Climatology,
1111 *Journal of Advances in Modeling Earth Systems*, 12(8), doi:10.1029/2019ms002025, 2020.

1112
1113 Kim, Y., Moorcroft, P. R., Aleinov, I., Puma, M. J. and Kiang, N. Y.: Variability of phenology
1114 and fluxes of water and carbon with observed and simulated soil moisture in the Ent Terrestrial
1115 Biosphere Model (Ent TBM version 1.0.1.0.0), *Geoscientific Model Development*, 8(12), 3837–
1116 3865, doi:10.5194/gmd-8-3837-2015, 2015.

1117

1118 Koch, D., Schmidt, G. A. and Field, C. V.: Sulfur, sea salt, and radionuclide aerosols in GISS
 1119 ModelE, *Journal of Geophysical Research*, 111(D6), doi:10.1029/2004jd005550, 2006.
 1120

1121 Koster, R. D., Guo, Z., Yang, R., Dirmeyer, P. A., Mitchell, K. and Puma, M. J.: On the Nature
 1122 of Soil Moisture in Land Surface Models, *Journal of Climate*, 22(16), 4322–4335,
 1123 doi:10.1175/2009jcli2832.1, 2009.
 1124

1125 Li, W., Wang, Y., Flynn, J., Griffin, R. J., Guo, F. and Schnell, J. L.: Spatial Variation of Surface
 1126 O₃ Responses to Drought Over the Contiguous United States During Summertime: Role of
 1127 Precursor Emissions and Ozone Chemistry, *Journal of Geophysical Research: Atmospheres*,
 1128 127(1), doi:10.1029/2021jd035607, 2022.
 1129

1130 Loreto, F. and Sharkey, T. D.: A gas-exchange study of photosynthesis and isoprene emission in
 1131 *Quercus rubra* L., *Planta*, 182(4), 523–531, doi:10.1007/bf02341027, 1990.
 1132

1133 Miller, R. L., Cakmur, R. V., Perlwitz, J., Geogdzhayev, I. V., Ginoux, P., Koch, D., Kohfeld, K.
 1134 E., Prigent, C., Ruedy, R., Schmidt, G. A. and Tegen, I.: Mineral dust aerosols in the NASA
 1135 Goddard Institute for Space Sciences ModelE atmospheric general circulation model, *Journal of*
 1136 *Geophysical Research*, 111(D6), doi:10.1029/2005jd005796, 2006.
 1137

1138 Miller, R. L., Schmidt, G. A., Nazarenko, L. S., Bauer, S. E., Kelley, M., Ruedy, R., Russell, G.
 1139 L., Ackerman, A. S., Aleinov, I., Bauer, M., Bleck, R., Canuto, V., Cesana, G., Cheng, Y.,
 1140 Clune, T. L., Cook, B. I., Cruz, C. A., Del Genio, A. D., Elsaesser, G. S., Faluvegi, G., Kiang, N.
 1141 Y., Kim, D., Lacis, A. A., Leboissetier, A., Legrande, A. N., Lo, K. K., Marshall, J., Matthews,
 1142 E. E., Mcdermid, S., Mezuman, K., Murray, L. T., Oinas, V., Orbe, C., Pérez García-Pando, C.,
 1143 Perlwitz, J. P., Puma, M. J., Rind, D., Romanou, A., Shindell, D. T., Sun, S., Tausnev, N.,
 1144 Tsigaridis, K., Tselioudis, G., Weng, E., Wu, J. and Yao, M.: CMIP6 Historical Simulations
 1145 (1850–2014) With GISS-E2.1, *Journal of Advances in Modeling Earth Systems*, 13(1),
 1146 doi:10.1029/2019ms002034, 2021.
 1147

1148 Mishra, A. K. and V. Sinha (2020). "Emission drivers and variability of ambient isoprene,
 1149 formaldehyde and acetaldehyde in north-west India during monsoon season." *Environmental*
 1150 *Pollution* **267**: 115538.
 1151

1152 Müller, J.-F., Stavrakou, T., Wallens, S., De Smedt, I., Van Roozendaal, M., Potosnak, M. J.,
 1153 Rinne, J., Munger, B., Goldstein, A. and Guenther, A. B.: Global isoprene emissions estimated
 1154 using MEGAN, ECMWF analyses and a detailed canopy environment model, *Atmospheric*
 1155 *Chemistry and Physics*, 8(5), 1329–1341, doi:10.5194/acp-8-1329-2008, 2008.
 1156

1157 Monson, R. K., Weraduwege, S. M., Rosenkranz, M., Schnitzler, J.-P. and Sharkey, T. D.: Leaf
 1158 isoprene emission as a trait that mediates the growth-defense tradeoff in the face of climate
 1159 stress, *Oecologia*, 197(4), 885–902, doi:10.1007/s00442-020-04813-7, 2021.
 1160

1161 Ochsner, T. E., Cosh, M. H., Cuenca, R. H., Dorigo, W. A., Draper, C. S., Hagimoto, Y., Kerr,
 1162 Y. H., Larson, K. M., Njoku, E. G., Small, E. E. and Zreda, M.: State of the Art in Large-Scale

1163 Soil Moisture Monitoring, *Soil Science Society of America Journal*, 77(6), 1888–1919,
1164 doi:10.2136/sssaj2013.03.0093, 2013.
1165
1166 Opacka, B., Müller, J.-F., Stavrakou, T., Bauwens, M., Sindelarova, K., Markova, J. and
1167 Guenther, A. B.: Global and regional impacts of land cover changes on isoprene emissions
1168 derived from spaceborne data and the MEGAN model, *Atmospheric Chemistry and Physics*,
1169 21(11), 8413–8436, doi:10.5194/acp-21-8413-2021, 2021.
1170
1171 Pegoraro, E., Rey, A., Greenberg, J., Harley, P., Grace, J., Malhi, Y. and Guenther, A.: Effect of
1172 drought on isoprene emission rates from leaves of *Quercus virginiana* Mill., *Atmospheric*
1173 *Environment*, 38(36), 6149–6156, doi:10.1016/j.atmosenv.2004.07.028, 2004.
1174
1175 Potosnak, M. J., Lestourgeon, L., Pallardy, S. G., Hosman, K. P., Gu, L., Karl, T., Geron, C. and
1176 Guenther, A. B.: Observed and modeled ecosystem isoprene fluxes from an oak-dominated
1177 temperate forest and the influence of drought stress, *Atmospheric Environment*, 48, 314–322,
1178 doi:10.1016/j.atmosenv.2013.11.055, 2014.
1179
1180 Rasmusson, L. M., Gullström, M., Gunnarsson, P. C. B., George, R. and Björk, M.: Estimation
1181 of a whole plant Q10 to assess seagrass productivity during temperature shifts, *Scientific*
1182 *Reports*, 9(1), doi:10.1038/s41598-019-49184-z, 2019.
1183
1184 Rosenstiel, T. N., Potosnak, M. J., Griffin, K. L., Fall, R. and Monson, R. K.: Increased CO₂
1185 uncouples growth from isoprene emission in an agriforest ecosystem, *Nature*, 421(6920), 256–
1186 259, doi:10.1038/nature01312, 2003.
1187
1188 Schnell, J. L., Holmes, C. D., Jangam, A. and Prather, M. J.: Skill in forecasting extreme ozone
1189 pollution episodes with a global atmospheric chemistry model, *Atmospheric Chemistry and*
1190 *Physics*, 14(15), 7721–7739, doi:10.5194/acp-14-7721-2014, 2014.
1191
1192 Seco, R., Karl, T., Guenther, A., Hosman, K. P., Pallardy, S. G., Gu, L., Geron, C., Harley, P.
1193 and Kim, S.: Ecosystem-scale volatile organic compound fluxes during an extreme drought in a
1194 broadleaf temperate forest of the Missouri Ozarks (central USA), *Global Change Biology*,
1195 21(10), 3657–3674, doi:10.1111/gcb.12980, 2015.
1196
1197 Seleiman, M. F., Al-Suhaibani, N., Ali, N., Akmal, M., Alotaibi, M., Refay, Y., Dindaroglu, T.,
1198 Abdul-Wajid, H. H. and Battaglia, M. L.: Drought Stress Impacts on Plants and Different
1199 Approaches to Alleviate Its Adverse Effects, *Plants*, 10(2), 259, 2021.
1200
1201 Sharkey, T. D. and Singaas, E. L.: Why plants emit isoprene, *Nature*, 374(6525), 769–769,
1202 doi:10.1038/374769a0, 1995.
1203
1204 Sharkey, T. D., Wiberley, A. E. and Donohue, A. R.: Isoprene Emission from Plants: Why and
1205 How, *Annals of Botany*, 101(1), 5–18, doi:10.1093/aob/mcm240, 2007.
1206
1207 Shindell, D. T., Pechony, O., Voulgarakis, A., Faluvegi, G., Nazarenko, L., Lamarque, J.-F.,
1208 Bowman, K., Milly, G., Kovari, B., Ruedy, R. and Schmidt, G. A.: Interactive ozone and

1209 methane chemistry in GISS-E2 historical and future climate simulations, *Atmospheric Chemistry*
1210 *and Physics*, 13(5), 2653–2689, doi:10.5194/acp-13-2653-2013, 2013.

1211

1212 Sindelarova, K., Granier, C., Bouarar, I., Guenther, A., Tilmes, S., Stavrakou, T., Müller, J.-F.,
1213 Kuhn, U., Stefani, P. and Knorr, W.: Global data set of biogenic VOC emissions calculated by
1214 the MEGAN model over the last 30 years, *Atmospheric Chemistry and Physics*, 14(17), 9317–
1215 9341, doi:10.5194/acp-14-9317-2014, 2014.

1216

1217 Singaas, E. L. and Sharkey, T. D.: The effects of high temperature on isoprene synthesis in oak
1218 leaves, *Plant, Cell & Environment*, 23(7), 751–757, doi:10.1046/j.1365-3040.2000.00582.x,
1219 2000.

1220

1221 Tawfik, A. B., Stöckli, R., Goldstein, A., Pressley, S. and Steiner, A. L.: Quantifying the
1222 contribution of environmental factors to isoprene flux interannual variability, *Atmospheric*
1223 *Environment*, 54, 216–224, doi:10.1016/j.atmosenv.2012.02.018, 2012.

1224

1225 Tsigaridis, K., Koch, D. and Menon, S.: Uncertainties and importance of sea spray composition
1226 on aerosol direct and indirect effects, *Journal of Geophysical Research: Atmospheres*, 118(1),
1227 220–235, doi:10.1029/2012jd018165, 2013.

1228

1229 Unger, N., Harper, K., Zheng, Y., Kiang, N. Y., Aleinov, I., Arneth, A., Schurgers, G.,
1230 Amelynck, C., Goldstein, A., Guenther, A., Heinesch, B., Hewitt, C. N., Karl, T., Laffineur, Q.,
1231 Langford, B., A. McKinney, K., Misztal, P., Potosnak, M., Rinne, J., Pressley, S., Schoon, N. and
1232 Serça, D.: Photosynthesis-dependent isoprene emission from leaf to planet in a global carbon-
1233 chemistry-climate model, *Atmospheric Chemistry and Physics*, 13(20), 10243–10269,
1234 doi:10.5194/acp-13-10243-2013, 2013.

1235

1236 Van Marle, M. J. E., Kloster, S., Magi, B. I., Marlon, J. R., Daniau, A.-L., Field, R. D., Arneth,
1237 A., Forrest, M., Hantson, S., Kehrwald, N. M., Knorr, W., Lasslop, G., Li, F., Mangeon, S., Yue,
1238 C., Kaiser, J. W. and Van Der Werf, G. R.: Historic global biomass burning emissions for
1239 CMIP6 (BB4CMIP) based on merging satellite observations with proxies and fire models (1750–
1240 2015), *Geoscientific Model Development*, 10(9), 3329–3357, doi:10.5194/gmd-10-3329-2017,
1241 2017.

1242

1243 Vermote, Eric; NOAA CDR Program. (2019): NOAA Climate Data Record (CDR) of AVHRR
1244 Leaf Area Index (LAI) and Fraction of Absorbed Photosynthetically Active Radiation (FAPAR),
1245 Version 5. LAI 2012. NOAA National Centers for Environmental Information.
1246 <https://doi.org/10.7289/V5TT4P69>. Accessed July 25, 2022.

1247

1248 Vicente-Serrano, S. M., Beguería, S. and López-Moreno, J. I.: A Multiscalar Drought Index
1249 Sensitive to Global Warming: The Standardized Precipitation Evapotranspiration Index, *Journal*
1250 *of Climate*, 23(7), 1696–1718, doi:10.1175/2009jcli2909.1, 2010.

1251

1252 Wang, P., Liu, Y., Dai, J., Fu, X., Wang, X., Guenther, A. and Wang, T.: Isoprene Emissions
1253 Response to Drought and the Impacts on Ozone and SOA in China, *Journal of Geophysical*
1254 *Research: Atmospheres*, 126(10), doi:10.1029/2020jd033263, 2021.

1255
1256 Wang, Y., Xie, Y., Dong, W., Ming, Y., Wang, J. and Shen, L.: Adverse effects of increasing
1257 drought on air quality via natural processes, *Atmospheric Chemistry and Physics*, 17(20),
1258 12827–12843, doi:10.5194/acp-17-12827-2017, 2017.
1259
1260 Wang, P., Holloway, T., Bindl, M., Harkey, M. and De Smedt, I.: Ambient Formaldehyde over
1261 the United States from Ground-Based (AQS) and Satellite (OMI) Observations, *Remote Sensing*,
1262 14(9), 2191, doi:10.3390/rs14092191, 2022.
1263
1264 Wells, K. C., Millet, D. B., Payne, V. H., Deventer, M. J., Bates, K. H., De Gouw, J. A., Graus,
1265 M., Warneke, C., Wisthaler, A. and Fuentes, J. D.: Satellite isoprene retrievals constrain
1266 emissions and atmospheric oxidation, *Nature*, 585(7824), 225–233, doi:10.1038/s41586-020-
1267 2664-3, 2020.
1268
1269 Zhao, Z., Wang, Y., Qin, M., Hu, Y., Xie, Y. and Russell, A. G.: Drought Impacts on Secondary
1270 Organic Aerosol: A Case Study in the Southeast United States, *Environmental Science &*
1271 *Technology*, 53(1), 242–250, doi:10.1021/acs.est.8b04842, 2019.
1272
1273 Zhu, L., Jacob, D. J., Kim, P. S., Fisher, J. A., Yu, K., Travis, K. R., Mickley, L. J., Yantosca, R.
1274 M., Sulprizio, M. P., De Smedt, I., González Abad, G., Chance, K., Li, C., Ferrare, R., Fried, A.,
1275 Hair, J. W., Hanisco, T. F., Richter, D., Jo Scarino, A., Walega, J., Weibring, P. and Wolfe, G.
1276 M.: Observing atmospheric formaldehyde (HCHO) from space: validation and intercomparison
1277 of six retrievals from four satellites (OMI, GOME2A, GOME2B, OMPS) with SEAC4RS
1278 aircraft observations over the southeast US, *Atmospheric Chemistry and Physics*, 16(21), 13477–
1279 13490, doi:10.5194/acp-16-13477-2016, 2016.
1280
1281 Zhu, L., Mickley, L. J., Jacob, D. J., Marais, E. A., Sheng, J., Hu, L., Abad, G. G. and Chance,
1282 K.: Long-term (2005-2014) trends in formaldehyde (HCHO) columns across North America as
1283 seen by the OMI satellite instrument: Evidence of changing emissions of volatile organic
1284 compounds, *Geophysical Research Letters*, 44(13), 7079–7086, doi:10.1002/2017gl073859,
1285 2017.
1286
1287 Zhu, J., Penner, J. E., Lin, G., Zhou, C., Xu, L. and Zhuang, B.: Mechanism of SOA formation
1288 determines magnitude of radiative effects, *Proceedings of the National Academy of Sciences*,
1289 114(48), 12685–12690, doi:10.1073/pnas.1712273114, 2017.